Hydrol. Earth Syst. Sci., 30, 6763–6787, 2026
https://doi.org/10.5194/hess-30-6763-2026
© Author(s) 2026. This work is distributed under
the Creative Commons Attribution 4.0 License.

Hydrology and Earth System Sciences
Open Access
EGU

Technical note: Evaluation of snow water equivalent from large-scale land-surface products over Italy

Gökhan Sarigil[1], **Mattia Neri**[1], **Francesco Avanzi**[2], **and Elena Toth**[1]

[1]Department of Civil, Chemical, Environmental, and Materials Engineering, University of Bologna, Bologna, Italy
[2]CIMA Research Foundation, University Campus of Savona, Savona, Italy

Correspondence: Mattia Neri (mattia.neri5@unibo.it)

Received: 29 April 2026 – Discussion started: 20 May 2026
Revised: 24 September 2026 – Accepted: 16 October 2026 – Published: 2 November 2026

Abstract. Snow water equivalent (SWE) is a critical hydrological variable for water resource management in mountainous regions, where seasonal snowpacks function as natural reservoirs regulating streamflow and water supply. While high-resolution, observation-constrained regional or national snow products provide reliable daily SWE estimates at fine spatial resolution (less than 1 km), their limited temporal coverage often restricts their use for long-term hydro-climatological studies. Large-scale land-surface products, in which SWE is derived from land-surface model simulations driven by atmospheric reanalyses or regional dynamical downscaling systems, provide multi-decadal coverage, but their reliability may be affected by biases in meteorological forcing, limited topographic representation, and simplified snow process parameterisation, requiring rigorous regional evaluation. This study evaluates the SWE estimates of three large-scale land-surface products, i.e., the global ERA5-Land, the European CERRA-Land, and the Italian VHR-REA_IT, against the national reference dataset IT-SNOW across Italy. The analysis combines grid-scale bias assessment of mean annual SWE and snow cover duration with temporal correlation analysis of daily SWE series, and is complemented by an evaluation of precipitation and temperature biases in each product, providing insight into how each product represents the atmospheric conditions governing snow accumulation and ablation and thereby supporting the interpretation of the identified SWE discrepancies. The results show clear regional differences in product performance, with no single product performing best across all metrics. ERA5-Land shows the strongest temporal correlation with IT-SNOW, but tends to overestimate mean annual SWE and snow cover duration in the Alps. CERRA-Land shows more moderate biases than ERA5-Land in the Italian Alps, but generally underestimates mean annual SWE across most subregions, where autumn and winter precipitation deficits in the forcing limit snow accumulation. Across the Apennines, both ERA5-Land and CERRA-Land tend to underestimate SWE and snow cover duration, particularly in the northern sectors. VHR-REA_IT shows widespread underestimation and the weakest temporal correspondence with IT-SNOW despite its finer grid spacing, which may be due to its fully coupled atmosphere–land architecture with no assimilation of meteorological observations. Overall, the results suggest that forcing biases explain a substantial part of the observed SWE discrepancies, although not all of them. This study provides useful insights for the use of SWE estimates from large-scale land-surface products in long-term hydro-climatological assessments over Italy and helps to understand whether the products can be used to evaluate snow dynamics in mountainous regions lacking high-quality benchmark estimates.

1 Introduction

Mountain snowpacks function as natural reservoirs, accumulating precipitation during colder months and gradually releasing it as meltwater during warmer seasons. This seasonal regulation sustains streamflow and water availability in snow-dependent regions, supporting ecosystems, agriculture, hydropower, and domestic water supply (Barnett et al., 2005; Immerzeel et al., 2020). As such, understanding the spatial and temporal distribution of snow is essential for water resource monitoring, streamflow forecasting, flood prediction,

and climate change diagnostics (Bormann et al., 2018; Viviroli et al., 2007).

Snow water equivalent (SWE), defined as the depth of water stored in the snowpack, represents the most direct link to mountain hydrology (King et al., 2020; Takala et al., 2011). However, obtaining reliable and spatially distributed estimates of SWE remains a persistent challenge. Ground-based approaches, including manual snow courses, snow pillows, passive gamma radiation sensors, and cosmic ray neutron sensors, provide valuable site-scale SWE observations through either direct weighing-based measurements or indirect physical inference. But their spatial coverage remains limited due to difficult terrain, adverse weather, and the prohibitive cost of establishing dense observation networks in mountain environments (Bales et al., 2006). These challenges are compounded by the highly variable spatial distribution of snow in mountainous terrain, where SWE can vary dramatically over short distances due to differences in elevation, slope, aspect, and wind exposure (Pflug et al., 2025; Pimentel et al., 2017; Sabetghadam et al., 2025). To overcome these limitations, several approaches have been developed to estimate SWE over large domains.

Satellite remote sensing substantially extends observational coverage beyond ground-based measurements, but current sensor classes still face important limitations for SWE estimation across diverse snow and landscape conditions. Optical sensors, such as MODIS snow cover products (Hall et al., 2002), are effective for mapping snow-covered area, yet they do not provide information on snow depth or SWE. Passive microwave sensors, including AMSR-E and AMSR2, can estimate SWE directly (Kelly, 2009), but their performance is constrained by coarse spatial resolution, signal saturation in deep snowpacks (Chang et al., 1987), and attenuation from forest canopy (Dong et al., 2005). Active microwave products, such as the Sentinel-1-derived C-SNOW dataset (Lievens et al., 2019), offer finer spatial resolution than passive sensors but retrieve snow depth rather than SWE and are mainly applicable under dry-snow conditions, because liquid water in the snowpack absorbs much of the radar signal (Mätzler, 1987; Mirza et al., 2025).

The combined limitations of ground-based measurements and satellite retrievals make it difficult to obtain spatially continuous and temporally consistent SWE estimates across large mountain domains. This challenge has motivated the development of gridded SWE products based on numerical modelling, with varying degrees of snow observation assimilation. High-resolution observation-constrained snow products, typically at ≤ 1 km resolution, are generated by integrating process-based snow modelling with the assimilation of ground-based and satellite snow observations to produce gridded SWE fields. Prominent examples include those developed for Italy (IT-SNOW, ~ 500 m; Avanzi et al., 2023), Switzerland (OSHD, up to ~ 250 m; Mott et al., 2023), the contiguous United States (SNODAS, ~ 1 km; NOHRSC, 2004), the Po River District (J-snow, ~ 500 m; Dall'Amico et al., 2025), the extratropical Andes (~ 180 m; Cortés and Margulis, 2017), High Mountain Asia (~ 500 m; Liu et al., 2021), and the western United States (~ 500 m; Fang et al., 2022). Despite their demonstrated reliability, the temporal and geographical coverage of these products varies widely, since it depends on the length of the assimilated observational records and on the design of each individual product. For example, while the Andes and western United States products, which assimilate fractional snow-covered area retrieved from the Landsat record, extend back to the mid-1980s, SNODAS and IT-SNOW begin in 2003 and 2010, respectively, and J-snow covers only the Po River District. Therefore, temporal and spatial coverage may limit the applicability of observation-constrained snow products for multi-decadal or large-scale studies.

Large-scale land-surface products, derived from atmospheric reanalyses and regional dynamical downscaling systems that provide continuous meteorological fields over multi-decadal periods, partially overcome the spatial and temporal limitations of observation-constrained snow products by providing internally consistent, gap-free spatiotemporal fields over broad domains. In these systems, SWE is simulated primarily by the snow scheme embedded within the land-surface model, driven by meteorological forcing and, in many cases, without direct assimilation of snow observations. The accuracy of the simulated snowpack is therefore strongly influenced by the quality of the meteorological forcing, which has been identified as a major source of error in snow simulations (Raleigh et al., 2015; Terzago et al., 2020), although its relative importance depends on the modelling framework and application (von Kaenel and Margulis, 2025). Beyond forcing quality, the structure of the snow scheme and the parameterisation of individual snow processes, such as albedo evolution, compaction, and liquid water retention, introduce an additional source of uncertainty (Cho et al., 2022; Günther et al., 2020). This highlights that rigorous validation is required before any land-surface product can be confidently applied for operational purposes.

Although previous studies have evaluated large-scale SWE products in other regions and confirmed that product performance varies with geographic and hydroclimatic setting (Brown et al., 2018; Broxton et al., 2016; Fang et al., 2023; Liu et al., 2022; Monteiro and Morin, 2023; Mudryk et al., 2025), no systematic evaluation of SWE estimates from large-scale land-surface products has yet been conducted across the whole of Italy. This gap is particularly relevant because the Italian Alps and Apennines are critical headwater regions for national water supply and have experienced marked recent declines in snowpack (Avanzi et al., 2024; Bocchiola and Diolaiuti, 2010), with direct implications for seasonal water availability in downstream basins (Montanari et al., 2023). This study addresses that gap by evaluating SWE estimates from three large-scale land-surface products against IT-SNOW (Avanzi et al., 2023), a high-resolution observation-constrained snow product assimilating dense in

situ and satellite snow observations and currently the most reliable gridded SWE reference available for Italy since 2010. The core goal of the evaluation is to assess the potential and limitations of these large-scale products and their underlying land-surface models and atmospheric forcing over the major mountain chains within Italy. The practical implications are twofold: on the national scale, given the limited temporal coverage of IT-SNOW, the results provide guidance for selecting the most suitable product for extending SWE records to prior decades and supporting long-term hydroclimatological assessments; on the continental and global scales, the findings may help characterise the reliability of these products in other hydrologically similar regions that lack high-quality benchmark estimates.

The Technical Note is structured as follows. Section 2 describes the study area. Section 3 presents the reference dataset, IT-SNOW, and the three evaluated products, including their atmospheric forcing and land-surface models. Section 4 describes the evaluation methodology. Section 5 presents and discusses the evaluation results in terms of mean annual SWE, snow cover duration, and temporal correlation of daily SWE. Section 6 summarises the main findings and their implications.

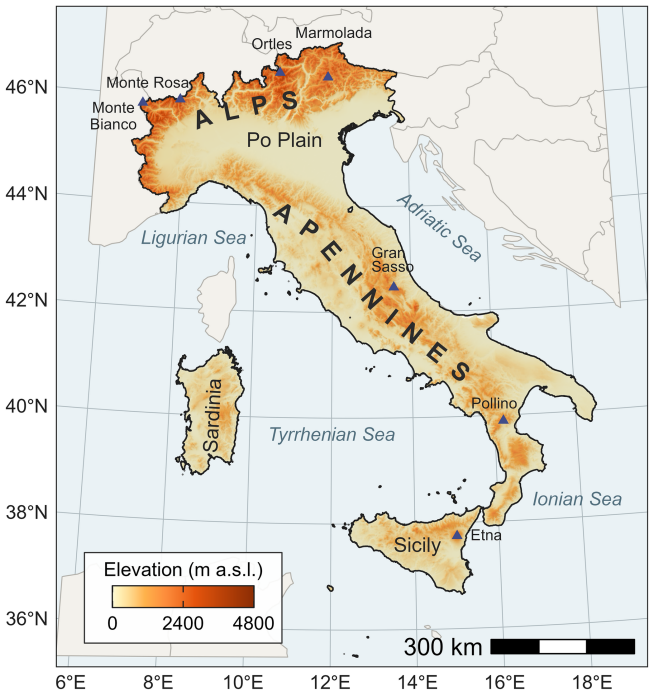


Figure 1. Topographic map of the study domain showing elevation (m a.s.l.).

2 Study area

The study area is Italy, characterised by sharp elevation contrasts where mountain ranges and coastlines combine to shape a great variety of hydrological and climatic conditions (Fig. 1). Elevation varies strongly across the country, from sea level along the extensive Mediterranean coastline to above 4000 m a.s.l (meter above sea level). across the highest mountain crests. Italian topography is dominated by two major mountain systems: the Alps, which arc along the northern border and represent the main area of seasonal snow storage and meltwater generation for northern Italy, and the Apennine chain, which forms the backbone of the peninsula and extends for about 1350 km to the Strait of Messina, continuing into northern Sicily. Marked relief also occurs on the major islands, Sardinia and Sicily.

The topographic contrasts described above translate into marked spatial gradients in climatic conditions and snow storage across Italy. Figure 2 summarises this variability through mean annual precipitation (panel a), mean annual temperature (panel b), and mean annual SWE (panel c), all computed as temporal averages of daily values over the study period from September 2010–August 2024. The precipitation and temperature fields are derived from SCIA (Sistema nazionale per la raccolta, elaborazione e diffusione di dati Climatologici di Interesse Ambientale; Desiato et al., 2007, 2011), a national gridded observational dataset, whereas SWE is derived from IT-SNOW (Avanzi et al., 2023), the high-resolution observation-constrained snow product for Italy that is here used as the reference SWE product. These datasets are used here to characterise the study area, while their full description and role in the evaluation are provided later in Sect. 3.1 for IT-SNOW and Sect. 4.2 for SCIA.

Figure 2 highlights the marked spatial variability of climate and snow conditions across Italy. Mean annual precipitation (panel a) reflects the influence of orography (Frei and Schär, 1998), with the highest values along the Alpine arc and the northern Apennines, particularly in the Ligurian sector, where moisture from the Mediterranean is enhanced by uplift (Miglietta and Davolio, 2022), while lower values occur across lowland areas and the major islands. Mean annual temperature (panel b) follows the main elevation gradient, with the coldest conditions in the highest Alpine sectors, intermediate values along the Apennine ridge, and the warmest conditions in coastal areas, plains, and the islands. Together, these precipitation and temperature patterns shape the spatial distribution of mean annual SWE (panel c). The highest SWE values occur in the Alps, where high elevations maintain colder conditions, increase the fraction of precipitation falling as snow, and delay melt. In the Apennines, SWE is generally lower and more spatially heterogeneous, despite moderate precipitation in several sectors, because milder conditions limit snow accumulation and persistence. Nonetheless, the highest massifs of the central Apennines sustain seasonal, though highly variable, snow cover (De Bellis et al., 2010; AINEVA, 2023). In the plains and coastal areas, mean annual SWE is close to zero. Overall, these contrasts, from the larger and more persistent Alpine snowpacks

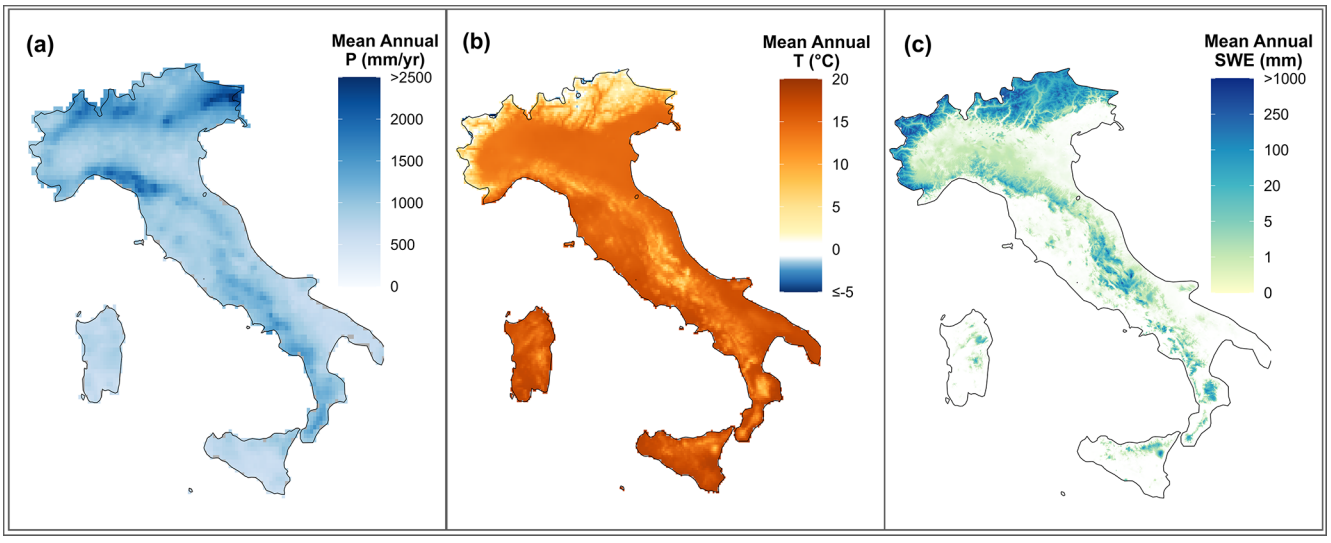


Figure 2. Climatic and snow regime characteristics of the study area for the period 2010–2024: **(a)** mean annual precipitation and **(b)** mean annual temperature from the SCIA observational dataset, and **(c)** mean annual snow water equivalent from the IT-SNOW reference dataset.

to the smaller and more intermittent Apennine snow cover, make Italy well suited for evaluating land-surface products across a wide range of snow regimes.

3 Datasets and product descriptions

3.1 Reference SWE dataset: IT-SNOW

IT-SNOW is a high-resolution, observation-constrained snow reanalysis for Italy, available from September 2010 onward, providing daily maps of SWE, snow depth, bulk snow density, and liquid water content at ~ 500 m spatial resolution (Avanzi et al., 2023). The reanalysis is generated retrospectively by rerunning the operational Snow Multidata Mapping and Modeling (S3M) chain for Italy over the historical period, constraining the estimates by using in situ and satellite snow data available for each date. S3M is a distributed cryospheric model developed by CIMA Research Foundation for the Italian Civil Protection Department (Avanzi et al., 2022).

Meteorological forcing is derived from a very dense network of automatic weather stations providing hourly precipitation, air temperature, relative humidity, and incoming shortwave radiation. Precipitation fields (~ 1 km resolution) are generated using a modified conditional merging approach that blends rain gauge observations with radar data through the GRISO algorithm (Bruno et al., 2021). Air temperature is spatialised through region-specific hourly linear regressions against elevation, fitted within meteorological homogeneous regions defined by the Italian Civil Protection. Relative humidity and incoming shortwave radiation are spatialised using inverse distance weighting. At each hourly time step, total precipitation is partitioned into rainfall and snowfall based on air temperature and relative humidity, which is more reliable than temperature alone (Zhang et al., 2017), following Froidurot et al. (2014).

S3M solves the snow mass balance using a single-layer scheme with hybrid temperature-index and radiation-driven melt, snow settling, liquid water outflow, and albedo evolution (Avanzi et al., 2022). The melt formulation follows Pellicciotti et al. (2005) in separating radiation- and temperature-driven components, but S3M modulates the coefficients of both components using mean air temperature over the preceding 10 d, providing a parsimonious proxy for snowpack cold content and thermal inertia (Avanzi et al., 2022). Glacier areas, identified from the Randolph Glacier Inventory v6.0 (Pfeffer et al., 2014), are handled separately within the model, so that the IT-SNOW SWE fields represent only seasonal snowpack.

The modelled snowpack is constrained by the daily assimilation of snow depth observations. These come from a network of ~ 350 ultrasonic sensors that follows the distribution of Italian snow resources and is therefore densest across the northern regions, particularly within the Po river basin. The point measurements are spatialised each day through multilinear regressions against elevation, slope, and aspect, fitted separately over 10 subdivisions of the territory that group areas of comparable snow climatology. The resulting fields are then trimmed to the observed snow line, using a blended snow-covered area map that combines Sentinel-2 (Main-Knorn et al., 2017), MODIS/VIIRS, and EUMETSAT H SAF H10 retrievals: pixels observed as snow-free are removed, so that the regressions do not extend snow onto bare ground. Conversion of the masked fields to SWE relies on the modelled snow density, whose spatial variability is considerably lower than that of snow depth (Mizukami and Perica, 2008).

The SWE fields obtained in this way are assimilated once per day through spatially distributed Newtonian relaxation, or nudging: at each grid cell the modelled SWE is corrected by a fraction of its departure from the observation-based estimate, and this fraction decreases with distance from the sensors. The procedure is confined to December–April, outside which the ultrasonic sensors may pick up the vegetation growing beneath them after melt-out and introduce spurious signals into the spatialised maps (Avanzi et al., 2023).

IT-SNOW has been evaluated against Sentinel-1-derived snow depth maps (C-SNOW; Lievens et al., 2019) over the period September 2016–April 2020, and against independent in situ snow depth and SWE measurements (Avanzi et al., 2023). The comparison against C-SNOW showed that IT-SNOW snow depth estimates were consistent with satellite-based snow data, with low mean bias across the evaluated mountain areas (mean bias: −10 mm; mean RMSE: 220 mm), and comparison against ground measurements confirmed that the dataset reconstructs seasonal snow accumulation and melt dynamics (RMSE: 300–600 mm for snow depth; 90–300 mm for SWE).

3.2 Evaluated large-scale land-surface products

The products evaluated in this study differ in both product architecture and the way observational information enters the modelling system. Because these structural differences directly affect how biases originate and propagate into the simulated SWE fields, understanding them provides the basis for interpreting the evaluation results. This requires distinguishing the role of the atmospheric component from that of the land-surface modelling component in each product.

Atmospheric reanalyses reconstruct past atmospheric conditions by reprocessing the historical observing record with a fixed numerical weather prediction model and data assimilation system (Baatz et al., 2021). The atmospheric model solves the governing equations for mass, momentum, and energy, advancing prognostic state variables such as air temperature, humidity, wind components, and surface pressure, which together describe the instantaneous state of the atmosphere. Data assimilation updates this model state, adjusting the prognostic variables to bring the analysed atmospheric state into closer agreement with available observations while maintaining consistency with the model dynamics (Kalnay, 2003). In conventional atmospheric reanalyses, precipitation and the turbulent fluxes of latent and sensible heat differ in nature from the prognostic state variables: they do not describe the atmosphere at an instant but represent transfers of mass and energy over a time interval, and are typically diagnosed from the evolving model state rather than analysed directly. They are generated by the model itself, with precipitation produced within the atmospheric column by the cloud microphysics and convection schemes, and the turbulent surface fluxes evaluated at the land–atmosphere interface from the model atmospheric state and the prescribed or simulated surface conditions (Betts et al., 1996).

Simulating SWE and other land-surface variables requires a land-surface model with dedicated schemes for snow, soil, and vegetation processes. Two main configurations are commonly used for running such a model: offline and coupled (Masson et al., 2013). In an offline configuration, the land-surface model is driven by meteorological forcing fields and does not return energy or moisture fluxes to the atmosphere. These forcing fields may come directly from a global atmospheric reanalysis or from a regional atmospheric model or reanalysis that dynamically downscales a larger-scale driving system to higher resolution (Giorgi and Mearns, 1999; Laprise et al., 2008). In a coupled configuration, the land-surface scheme is integrated within the atmospheric model, and the two components exchange energy, moisture, and momentum continuously (Betts et al., 1996). Such coupling allows land–atmosphere feedbacks to develop, but also permits biases in either component to propagate through the coupled system (Santanello et al., 2018). The main characteristics of the three evaluated products, including their atmospheric forcing source, land-surface model, and coupling configuration, are summarised in Table 1.

The fifth-generation ECMWF reanalysis ERA5 is the common upstream global reanalysis from which all three evaluated products derive their atmospheric information, though in different ways. ERA5 is produced within the Copernicus Climate Change Service based on the Integrated Forecasting System at approximately 31 km horizontal resolution (Hersbach et al., 2020). Its atmospheric state is constrained through a hybrid incremental four-dimensional variational data assimilation system (Courtier et al., 1994), in which observations are assimilated within 12 h windows using short-range forecasts as the background. The assimilated observing system includes surface stations, radiosondes, aircraft, ships, buoys, and a large volume of satellite radiances (Soci et al., 2024).

The differences in how each of the analysed products uses this common source are relevant for interpreting their SWE estimates: ERA5-Land is driven directly by ERA5 atmospheric forcing fields, CERRA-Land receives its forcing through the intermediate regional atmospheric reanalysis CERRA (Ridal et al., 2024), for which ERA5 provides lateral boundary conditions, and VHR-REA_IT uses ERA5 only as lateral boundary conditions within a fully coupled regional atmosphere–land system. The following sections describe each product in more detail, focusing on the atmospheric forcing chain and the snow scheme.

3.2.1 ERA5-Land

ERA5-Land is a global land-surface reanalysis produced by the European Centre for Medium-Range Weather Forecasts (ECMWF), providing land variables at approximately 9 km (0.1°) resolution from 1950 to near-present (Muñoz-Sabater

Table 1. Main characteristics of the large-scale land-surface products evaluated in this study.

Dataset	Spatial and temporal coverage	Resolution	Atmospheric model	Land-surface model	Produced by
ERA5-Land (Muñoz-Sabater et al., 2021)	Global, 1950–present	∼ 9 km, Hourly	IFS (ERA5 atmospheric forcing)	CHTESSEL	ECMWF/ Copernicus C3S
CERRA-Land (Verrelle et al., 2022)	Europe, 1984–present	5.5 km, 3 hourly	HARMONIE-ALADIN (CERRA atmospheric forcing)	SURFEX	ECMWF/ Copernicus C3S
VHR-REA_IT (Raffa et al., 2021)	Italy, 1981–present	∼ 2.2 km, Hourly	COSMO-CLM	TERRA-ML	CMCC

et al., 2021). The dataset is generated by running the CHTESSEL land-surface model (Balsamo et al., 2009) in offline mode, driven by atmospheric forcing derived from the ERA5 reanalysis (Hersbach et al., 2020).

To achieve the higher spatial resolution, the forcing fields are spatially downscaled from ERA5's ∼ 31 km grid to ERA5-Land's 9 km resolution. Precipitation is redistributed through linear interpolation from ERA5 to the 9 km grid, without any further correction, whereas temperature, humidity, and pressure from ERA5's lowest model level (approximately 10 m above the surface) are interpolated and corrected for elevation differences using daily lapse rates. Notably, the 2 m temperature is not directly downscaled from ERA5 but is computed internally by CHTESSEL from the surface energy balance: the model first solves for the skin temperature (i.e., the radiative temperature of the outermost surface) and then estimates the 2 m temperature by interpolating between this value and the elevation-corrected 10 m temperature.

CHTESSEL uses a single-layer bulk snow scheme (Dutra et al., 2010) that represents the entire snowpack as a single homogeneous layer with uniform temperature, density, and liquid water content. In ERA5-Land, liquid and solid precipitation are inherited from the ERA5 forcing and then interpolated to the 9 km ERA5-Land grid, so snowfall provides the solid input to the snow scheme rather than being diagnosed independently within the offline land-surface integration. The snow mass balance includes accumulation from snowfall, melting derived from the surface energy balance, and losses through sublimation. Snow density increases due to compaction and metamorphism, while snow albedo is reset toward its maximum after snowfall and then decays linearly during non-melting conditions and exponentially during melting conditions. The model lacks a dedicated glacier component; grid cells with more than 50 % ice cover are instead assigned a constant snow mass equivalent to 10 m water equivalent throughout the simulation.

ERA5-Land does not assimilate any land-surface observations; the only observational constraint enters the system through the assimilated atmospheric state of ERA5, from which the forcing fields are derived. Consequently, biases in the downscaled forcing fields can propagate into the SWE simulations without any observational correction at the land surface.

3.2.2 CERRA-Land

CERRA-Land provides European regional land-surface reanalysis at 5.5 km resolution and three-hourly frequency, covering September 1984 to present (Verrelle et al., 2022). The dataset is generated by running the SURFEX v8.1 land-surface model (SURFace EXternalisée; Masson et al., 2013) in offline mode, driven by meteorological forcing from the parent CERRA regional atmospheric reanalysis.

The CERRA atmospheric reanalysis (Ridal et al., 2024) is produced by running the HARMONIE-ALADIN regional atmospheric model (Bengtsson et al., 2017) at 5.5 km resolution over Europe, with ERA5 providing the lateral boundary conditions. Within the regional domain, CERRA develops its own atmospheric fields through higher-resolution dynamics and data assimilation, using conventional observations, satellite radiances, atmospheric motion vectors, and GNSS radio occultation data to constrain the atmospheric state. CERRA-Land adds the land-surface component to this atmospheric system at the same 5.5 km resolution. No land-surface observations are assimilated; however, before entering the land-surface model, the precipitation forcing undergoes a gauge-based correction.

Precipitation forcing in CERRA-Land is based on a daily gauge-corrected precipitation analysis produced with MESCAN and temporally disaggregated to 3 hourly resolution. Liquid and solid precipitation inputs are then derived from this corrected precipitation forcing through rain-snow partitioning following Froidurot et al. (2014), using the near-surface atmospheric fields provided by CERRA. CERRA-Land is therefore the only evaluated product whose forcing chain includes an explicit gauge-based correction of precipitation. Over Italy, however, the effectiveness of this adjustment is limited by the sparse gauge coverage available to MESCAN (Soci et al., 2016), so across much of the domain the precipitation forcing remains strongly dependent

on the CERRA atmospheric model output. The 2 m temperature, by contrast, is passed directly from the CERRA atmospheric reanalysis to CERRA-Land without re-computation, since HARMONIE-ALADIN already diagnoses 2 m temperature as a standard output of the atmospheric model. This differs from ERA5-Land, where the 2 m temperature is not taken from ERA5 but is derived internally by CHTESSEL through interpolation between the skin temperature solved from the surface energy balance and the elevation-corrected lowest-level atmospheric temperature.

SURFEX implements snow processes through the ISBA-ES (Interactions between Soil, Biosphere, and Atmosphere, Explicit Snow) multi-layer scheme (Boone and Etchevers, 2001; Vionnet et al., 2012), which divides the snowpack into 12 layers (Decharme et al., 2016). The scheme prognoses snow mass, density, and heat content for each layer, together with snow albedo; temperature and liquid water content are diagnosed from heat content. Layers are thinner near the snow surface and the snow–soil interface to resolve the diurnal cycle and snow–soil heat exchanges. The scheme simulates inter-layer heat transfer, liquid water percolation through a bucket approach, refreezing, and wind-driven densification, and computes an explicit snow surface energy balance governing snow warming and melt (Boone and Etchevers, 2001; Decharme et al., 2016). This multi-layer structure allows the representation of vertical temperature gradients and vertical variations in snowpack properties and processes that single-layer schemes such as CHTESSEL cannot explicitly resolve.

3.2.3 VHR-REA_IT

The Very High-Resolution Reanalysis for Italy (VHR-REA_IT) is a regional dynamical downscaling product for Italy produced by the Centro Euro-Mediterraneo sui Cambiamenti Climatici (CMCC), providing hourly variables at 2.2 km (0.02°) resolution for the period 1981 to near-present (Raffa et al., 2021). Unlike ERA5-Land and CERRA-Land, VHR-REA_IT is not generated through an offline land-surface simulation. Instead, the COSMO-CLM regional atmospheric model (Rockel et al., 2008) and the TERRA-ML land-surface model (Schrodin and Heise, 2001) run as a fully coupled system, exchanging fluxes of energy and moisture at every timestep.

Because VHR-REA_IT is produced with a fully coupled regional atmosphere–land modelling system, near-surface forcing fields are generated internally by the regional model rather than supplied through a separate offline forcing dataset. COSMO-CLM generates its own atmospheric fields at convection-permitting resolution, where deep convection is explicitly resolved while only shallow convection is parameterised (Doms et al., 2011). The atmospheric model is driven at its lateral boundaries by ERA5, with boundary conditions updated every 3 h; within the domain, the regional atmosphere evolves freely through its own dynamics (Loprieno et al., 2024). No observational data are assimilated within the regional domain, so the only observational constraint on VHR-REA_IT enters indirectly through the ERA5 lateral boundary conditions. The two-way coupling allows land–atmosphere feedbacks to develop, but also permits biases in either component to propagate through the coupled system. The atmospheric model provides the land-surface scheme with separate liquid and solid precipitation components, while their partitioning is determined within the atmospheric model.

Snow processes are handled by TERRA-ML, which represents the land surface through multiple soil layers but treats the snowpack as a single bulk reservoir. Snow accumulation increases the water content of this reservoir, while melt is computed from the coupled surface energy and water balance and contributes liquid water to the soil system. The model also accounts for phase changes between liquid and frozen water at the surface and within the soil (Doms et al., 2011).

4 Evaluation methodology

4.1 Data processing and SWE comparison setup

The comparison covers 14 snow-years from September 2010–August 2024. The start of this period is determined by the availability of the IT-SNOW reference dataset, while the end date is constrained by the SCIA observational dataset (Desiato et al., 2007, 2011), which is used for the complementary forcing evaluation described in Sect. 4.2 and, at the time of this analysis, is available through the end of 2024. The analysis is restricted to grid cells where IT-SNOW mean annual SWE exceeded 1 mm in at least one snow-year, thereby excluding cells with generally negligible SWE.

The SWE estimates were evaluated using three grid-scale indicators, each targeting a different aspect of snowpack representation:

- mean annual SWE, computed by averaging daily SWE over each snow-year and then across the full study period, quantifies the overall snow mass estimated by each product.

- snow cover duration (SCD), defined as the mean annual number of days with SWE at least 5 mm, characterises snowpack persistence; the 5 mm threshold was adopted to distinguish meaningful snow presence from marginal snow amounts, consistent with previous studies using the same threshold for snow-cover identification from SWE fields (Dawson et al., 2018; Di Marco et al., 2021; Jenicek et al., 2021; Matiu and Hanzer, 2022). It is to be underlined that, for consistency across datasets, SCD was derived directly from daily SWE values, for all products, rather than from the snow-cover-fraction fields (that are available in some of the products).

– the Pearson correlation coefficient between the daily SWE series of each product and the IT-SNOW reference, calculated at each grid cell over the study period, evaluates the ability of each product to reproduce day-to-day snowpack variability irrespective of magnitude bias.

The four datasets differ substantially in native resolution (IT-SNOW: ∼ 500 m; VHR-REA_IT: 2.2 km; CERRA-Land: 5.5 km; ERA5-Land: ∼ 9 km). Therefore, these indicators cannot be compared directly without spatial harmonisation. To enable a consistent quantitative intercomparison, the datasets were re-gridded to a common spatial framework (Lindsay et al., 2014; Mudryk et al., 2025). For mean annual SWE and SCD, annual indicator fields were first computed at each product's native resolution to preserve spatial gradients in complex terrain and to prevent the distortion of threshold-based statistics by prior spatial averaging (Matiu et al., 2021; Rajulapati et al., 2020). The resulting indicator fields were then re-gridded to the coarsest grid (ERA5-Land, ∼ 9 km) through first-order conservative remapping (Jones, 1999), and annual bias was calculated at each common-grid cell by subtracting the IT-SNOW value from the corresponding product value. These annual differences were averaged across all the snow-years to obtain the mean bias. Percentage bias was also computed as a complementary analysis and the resulting maps are shown in Supplement. Daily correlation required a different approach: because the Pearson coefficient must be computed from paired time series at matching grid cells, daily SWE fields were first re-gridded to the common 9 km grid through first-order conservative remapping, and the correlation was then computed pixel-wise over the full study period.

For each product and indicator, the statistical significance of mean annual SWE and SCD biases was assessed at each common-grid cell by applying a two-tailed Student's t-test to the time series of annual product–reference differences, testing whether their mean differed from zero. As discussed by Wilks (2016), interpreting numerous grid-cell tests without accounting for multiple testing can overstate the spatial extent of significant differences because some results are significant by chance alone. The resulting p-values were therefore evaluated using the Benjamini–Hochberg procedure (Benjamini and Hochberg, 1995), which controls the false discovery rate (FDR), defined as the expected proportion of false rejections among all rejected null hypotheses. The procedure was applied separately across the evaluated grid cells for each product and indicator. An FDR control level of 0.10 was adopted following Wilks (2016), who recommends using twice the target global significance level to obtain an approximately 0.05 global test level in fields with moderate to strong spatial correlation. Statistical significance is shown in Supplement to preserve the legibility of the main bias maps.

Finally, to obtain further insight into regional differences in product performance, the snow regime of each grid cell was also classified as seasonal or ephemeral according to snow persistence in the IT-SNOW reference. For each cell and snow-year, the longest sequence of consecutive days with SWE of at least 5 mm (the same threshold used for computing SCD) was identified, and its duration was averaged across all the snow-years. Following the 60 d persistence criterion (Sturm et al., 1995; Petersky and Harpold, 2018), cells with a mean duration of at least 60 d were classified as seasonal and the remaining cells as ephemeral. Since the classification serves as an interpretative aid rather than an evaluation result, the resulting regime map is provided in Appendix Fig. A1.

4.2 Complementary evaluation of atmospheric forcing

Precipitation and temperature are the main atmospheric controls on snow accumulation and ablation, and biases in these fields can contribute to discrepancies in simulated SWE (Monteiro and Morin, 2023; Terzago et al., 2020). Evaluating the precipitation and temperature fields associated with the three SWE products against an independent observational reference therefore provides useful context for interpreting the corresponding SWE discrepancies, although these discrepancies may also reflect other factors related to model structure and process representation.

The meteorological observational reference used for this purpose is SCIA (Desiato et al., 2007, 2011), maintained by the Italian Institute for Environmental Protection and Research (ISPRA). SCIA provides daily gridded precipitation at 10 km resolution from 1961 onwards and daily minimum and maximum 2 m air temperature at 5 km resolution from 1981 onwards, both derived from a high-density network of regional meteorological stations. The dataset has been widely adopted as a reference in Italian hydrological studies (e.g., Moccia et al., 2025; Sarigil et al., 2024), and its availability through the end of 2024 at the time of this analysis defines the end date of the study period adopted in this work.

For both the SCIA reference and each evaluated product, annual and seasonal precipitation depths and mean 2 m air temperatures were first calculated at native resolutions and then re-gridded to the common 9 km grid following the same procedure described in Sect. 4.1. Long-term mean annual and seasonal bias maps of each product against SCIA were thus calculated and used as a complementary diagnostic to support the interpretation of the SWE evaluation.

Given that a comprehensive standalone assessment of gridded meteorological products over Italy is not the main scope of this study, the mean annual and seasonal bias fields are presented in the Appendices rather than in the main text: Appendix B reports the mean annual biases (Fig. B1 for precipitation, Fig. B2 for temperature), and Appendix C reports the seasonal biases in precipitation, temperature, and SWE for each product (Fig. C1 for ERA5-Land, Fig. C2 for CERRA-Land, Fig. C3 for VHR-REA_IT). These figures are

referenced throughout Sect. 5 to support the interpretation of the SWE evaluation results.

In addition, the statistical significance of the mean annual precipitation and temperature biases was assessed using the same paired t test and false discovery rate (FDR) procedure described in Sect. 4.1, with SCIA as the reference. To preserve the legibility of the bias maps in Appendix Figs. B1 and B2, the results of the FDR-screening are shown in the corresponding expanded Supplement (Figs. S3 and S4).

5 Results and discussion

5.1 Mean annual SWE

The initial phase of the assessment is the comparison of the mean annual SWE estimates from each product. The results are presented in Fig. 3: figure's top row (panels a–d) displays the mean annual SWE from the IT-SNOW reference and the three land-surface products at their native resolution, allowing for a direct visualisation of their respective spatial distributions and magnitudes; in addition, to quantify the discrepancies from the reference data, the second row (panels e–g) presents bias maps calculated as the difference between each of the three land-surface products and the reference (Product – IT-SNOW), so that negative (red colour) values represent where the product underestimates the reference values and positive (blue colour) values represent an overestimation. For this comparison, the datasets resampled to the ERA5-Land resolution are used.

The three land-surface products (panels b–d) broadly reproduce the spatial distribution of SWE shown by the IT-SNOW reference (panel a), with the highest mean annual SWE values in the high Alps and along the Apennine ridge. The agreement, however, is largely confined to this overall pattern: the bias maps (panels e–g) show product–reference differences that are largest at high elevations, where mean annual SWE itself is the greatest, and that differ in sign among the products. Figure S1 presents an expanded version of this figure, adding percentage-bias panels and marking the cells whose biases are not significant after false discovery rate (FDR) screening. Where reference SWE is substantial, the percentage-bias panels largely mirror the absolute-bias pattern; where it is small, however, even small absolute differences can yield large percentage biases, which should therefore be interpreted with caution (Fig. S1, panels h–j). Across all products, cells with non-significant biases are generally confined to areas with the smallest bias values, whereas large biases are statistically significant (Fig. S1, panels e–g). Overall, this provides confidence in the validity of the mean SWE bias analysis, as the most prominent discrepancies prove to be statistically robust.

Considering the mean annual SWE estimates in more detail, we note that the coarse spatial resolution of ERA5-Land smooths out the high spatial variability of SWE (panel b). The bias map (panel e) shows large positive biases over much of the high Alpine region, alongside some localised negative values, whereas the Apennines and lowlands show widespread underestimation. The concentration of the overestimation in the highest mountain areas is consistent with what has been reported by Kouki et al. (2023), who attributed the ERA5-Land overestimation (150 %–200 %) of the spring SWE over the entire Northern Hemisphere mainly to excessively high values in the major mountain regions. The comparison of the meteorological forcing at seasonal scale (Fig. C1) shows that ERA5-Land exhibits positive winter precipitation biases together with negative winter temperature biases across the Alps, strongest over the north-western sector (Fig. C1, panels b and f), in agreement with Cavalleri et al. (2024a, b), Dalla Torre et al. (2024), and Sarigil et al. (2024). The co-occurrence of higher precipitation and lower temperatures in winter is consistent with enhanced snow accumulation and with positive SWE biases that persist into spring (Fig. C1, panels i–k). However, another potential explanation for such biases was given by Orsolini et al. (2019), who identified the discontinuation of snow-cover assimilation from the Interactive Multisensor Snow and Ice Mapping System (IMS) above 1500 m a.s.l. as a possible further contributor to high-elevation snow biases in ERA5 over the Tibetan Plateau, since the simulated snow cover at these elevations is no longer corrected by observed snow cover. The same restriction applies over the Alps, where excessive snow cover in ERA5 could increase surface albedo, artificially lowering near-surface temperatures; these cold biases could then be propagated into ERA5-Land, which relies on ERA5 meteorology as its atmospheric forcing. Moreover, snow–albedo interactions could also reinforce the positive SWE bias within ERA5-Land itself: within CHTESSEL, an excessive snowpack could prolong snow cover and maintain a higher surface albedo, reducing absorbed shortwave radiation and the energy available for melt, thereby further delaying snow depletion. In the Apennines, where snow is predominantly ephemeral and seasonal snow cells are largely confined to the highest elevations and most extensive over the central massifs (Fig. A1), the relationship between SWE biases and seasonal forcing biases is less straightforward. In the northern Apennines, the negative SWE bias is mainly consistent with a precipitation deficit rather than with temperature biases: both autumn and winter precipitation are underestimated, limiting snow accumulation from the onset of the season, whereas later anomalies are too weak or too late to offset the winter deficit (Fig. C1, panels a–d). In the central Apennines, however, the seasonal forcing biases do not readily explain the negative SWE bias: winter precipitation biases are near-neutral to weakly positive and winter temperature biases are negative (Fig. C1, panels b and f), conditions that would favour rather than suppress snow accumulation. This apparent inconsistency may reflect factors not resolved by the seasonal precipitation and temperature averages, including differences in precipitation-phase estimation, the limited

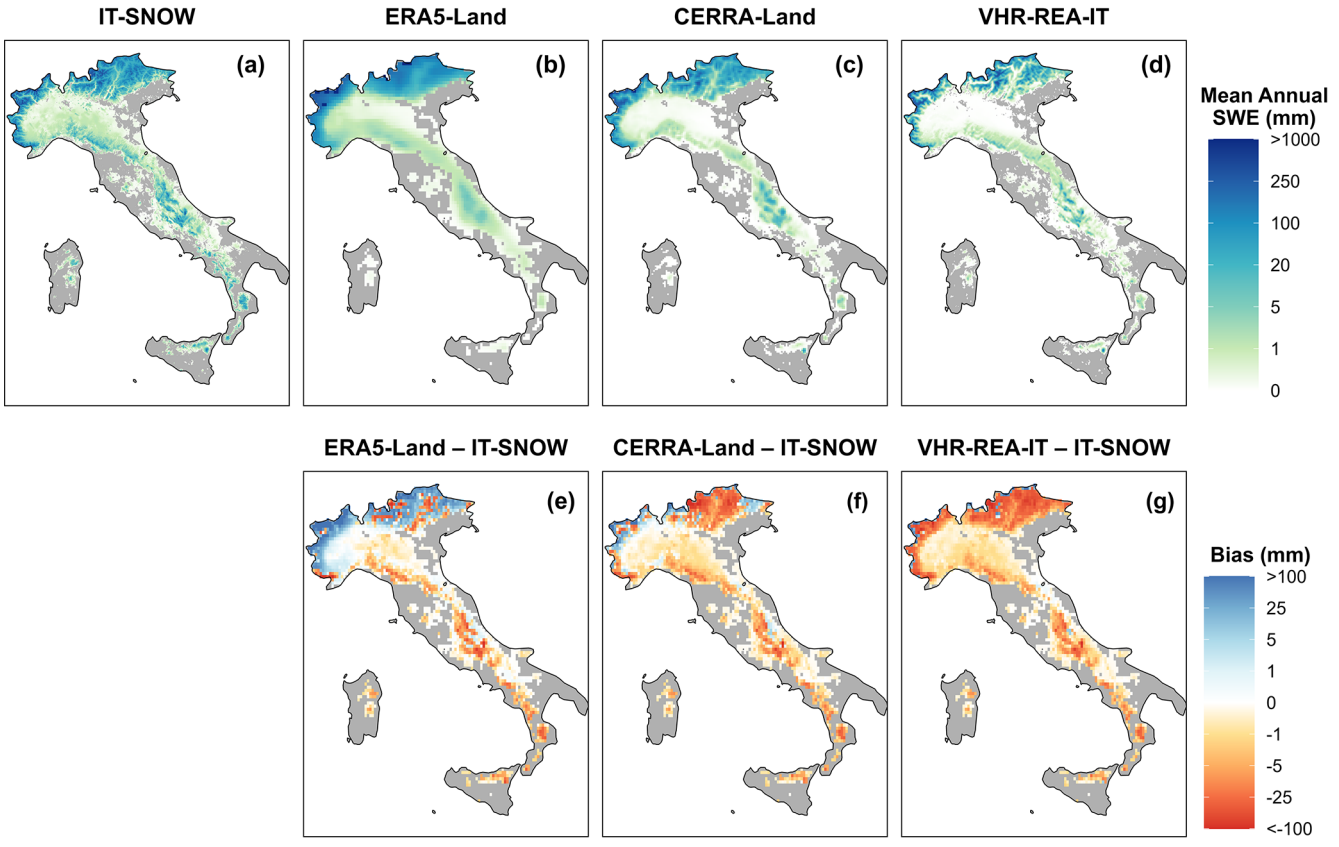


Figure 3. Comparison of mean annual snow water equivalent (SWE) for the period September 2010–August 2024. **(a–d)** Mean annual SWE maps for the IT-SNOW reference dataset and the three land-surface products at their native resolutions. **(e–g)** Spatial bias maps (Product – IT-SNOW) resampled to the common 9 km grid.

representation of the high-elevation massifs on the 9 km grid, and differences in the representation of snow processes such as ablation. Ablation, in particular, can be relevant even during the accumulation season: in evaluations of ERA5-Land and other global products in High Mountain Asia (Liu et al., 2022) and in the western United States and the Andes (Fang et al., 2023), accumulation-season snow losses contributed to inter-product differences in SWE estimation.

CERRA-Land demonstrates an improvement in reproducing the spatial variability of mean annual SWE compared to ERA5-Land, thanks to its finer 5.5 km grid spacing (Fig. 3, panel c). However, despite this improved spatial detail, annual SWE remains negatively biased in most regions, with some localised exceptions (panel f). In the Alps, unlike ERA5-Land which produces marked overestimation due to combined, strong and spatially coherent precipitation and temperature biases, CERRA-Land SWE is influenced by an overall weak underestimation of temperature during the snow season (Fig. C2, panels e–g) and a much more varying pattern of precipitation biases (Fig. C2, panels a–c). In the central and eastern Alps, autumn precipitation bias is scattered and changes across the valleys (Fig. C2, panel a), while in winter it is overall weakly negative (Fig. C2, panel b). Such a forcing pattern only partially explains the strong negative SWE bias in the same region, since the weak cold bias would favour rather than suppress snow accumulation and retention. This suggests that the observed deficit may reflect not only forcing errors but also processes internal to the snow modelling chain, although dedicated process-level diagnostics would be required to identify the specific mechanisms involved. The main Alpine exception is the northwestern Alps, where positive autumn–winter precipitation biases (Fig. C2, panels a–b) and colder conditions (Fig. C2, panels e–f) produce the only spatially coherent patches of positive SWE bias, although the cell-level pattern remains heterogeneous. However, interpretation of the SWE pattern in areas very close to the national border should nevertheless remain cautious since the reference datasets are less robust there: IT-SNOW assimilates fewer observations (Avanzi et al., 2023), and SCIA does not extend beyond the national border; in addition, gauge station density is also limited in such high-elevation areas. Across the Apennine chain, instead, the attribution is more direct: precipitation deficit is strongest during autumn and winter, especially in the north, leading to negative SWE biases during the main accumulation season despite the overall weak cold bias.

VHR-REA_IT exhibits the most spatially widespread negative SWE biases among the evaluated products, despite having the highest spatial resolution (~ 2.2 km) (Fig. 3, panels d and g). A strong negative SWE bias characterises much of the domain, although some high-elevation Alpine areas show locally positive anomalies during the early accumulation season (Fig. C3, panels i–j). The joint seasonal analysis reveals a seasonal asymmetry in the temperature bias, with a cold bias in winter transitioning to a strong warm bias in summer (Fig. C3, panels f and h), consistent with documented evaluations of the COSMO-CLM atmospheric fields over Italy (Adinolfi et al., 2023; Cavalleri et al., 2024a; Loprieno et al., 2024; Raffa et al., 2021). However, the seasonal meteorological forcing does not fully account for the SWE underestimation in several subregions. In the Alps, winter precipitation is generally overestimated and winter temperatures are colder than the reference (Fig. C3, panels b and f), conditions that should favour snow accumulation, yet SWE bias remains negative in all three Alpine subregions. Similarly, in the central Apennines, precipitation becomes weakly positive in winter while temperatures remain below the reference, yet SWE bias remains negative during the accumulation season (Fig. C3, panels i–k). Only in the northern Apennines do autumn–winter precipitation deficits provide a more direct explanation, although the persistence of negative SWE bias beyond winter suggests that precipitation deficit alone is insufficient to explain the full anomaly. The persistence of negative SWE biases under autumn–winter forcing conditions that would otherwise favour snow accumulation points to structural factors in the modelling chain. Unlike ERA5-Land and CERRA-Land, which are offline simulations driven by observationally constrained reanalysis forcing, VHR-REA_IT is a free-running dynamical downscaling in which COSMO-CLM and its land-surface scheme TERRA-ML operate as a fully coupled atmosphere–land system (Raffa et al., 2021), with no observations assimilated within the regional domain. Any initial negative SWE perturbation generated within this configuration, whether originating in the snow scheme structure, in model parameters, or in the internal forcing, can then be reinforced rather than corrected by the coupled atmosphere and land components: a reduction in simulated SWE lowers surface albedo, warms the lower boundary layer, and promotes further melt through land–atmosphere feedbacks (Santanello et al., 2018) that are not represented in the same two-way form in the offline configurations of the other two products. Finer resolution and two-way coupling therefore do not by themselves guarantee more accurate SWE estimates, underscoring the importance of observational constraints in high-resolution applications (Fang et al., 2023).

5.2 Snow cover duration

Beyond mean annual SWE magnitudes, snow cover duration (SCD), defined in Sect. 4.1 as the mean annual number of days with SWE at least 5 mm, provides complementary insights into snowpack temporal dynamics. SCD helps to better capture the integrated effects of meteorological and topographic factors, including temperature regimes, precipitation patterns, elevation, and energy balance processes, that collectively determine snow persistence. As a diagnostic variable, we used SCD for assessing the performance of the evaluated products across the complete seasonal cycle, as it integrates cumulative effects of biases in both accumulation and melting processes that may not be evident in mean SWE comparisons. Analogously to Fig. 3, Fig. 4 presents the spatial distribution of mean annual SCD for each dataset (panels a–d) at their native resolution and the corresponding biases relative to IT-SNOW (panels e–g) on the common resampled 9 km grid.

The SCD maps (Fig. 4, top panels a–d) confirm a common elevation-dependent spatial pattern across the country, consistent with mean annual SWE in Fig. 3. However, the bias analysis (bottom panels e–g) shows patterns that partially differ from the mean annual SWE biases (Fig. 3), indicating that biases in total snow mass do not always correspond to biases in snow cover persistence. Similarly to what showed for mean SWE bias, Fig. S2 complements these maps with percentage-bias panels and marking the cells whose biases are not significant after FDR screening. In the percentage-bias panels, the largest relative biases generally occur in lowland, southern and insular cells, where reference SCD is short (Fig. S2, panels h–j). As for mean annual SWE, the largest SCD biases are generally statistically significant, whereas non-significant cells mainly occur where biases are the smallest (Fig. S2, panels e–g).

ERA5-Land (panel e) displays a spatially heterogeneous SCD bias pattern that broadly mirrors the mean annual SWE biases (Fig. 3, panel e), with overestimation concentrated in the Alps and predominantly negative biases across the Apennines and southern Italy. Over the Alps, the positive SCD bias is strongest and most spatially coherent in the north-western sector, extending across the high-elevation areas where mean annual SCD is already longest, and weakens progressively towards the central and eastern sectors. This overestimation is consistent with the broader literature, which identifies prolonged snow cover as a characteristic bias of ERA5-Land over high mountain areas (Kouki et al., 2023; Monteiro and Morin, 2023). Over the European Alps specifically, Monteiro and Morin (2023) found ERA5-Land exhibiting the strongest and most spatially extensive SCD overestimation among all evaluated datasets when compared against MODIS satellite observations, with the largest discrepancies occurring at the melt-out date. Urraca and Gobron (2023), evaluating ERA5-Land against ground stations in the Northern Hemisphere, attributed the systematic positive SCD bias to the tendency of the CHTESSEL land-surface model to overestimate snow depth, likely due to excessive snowfall in the forcing. As discussed in Sect. 5.1, the combination of overestimated precipitation and persistent temperature underesti-

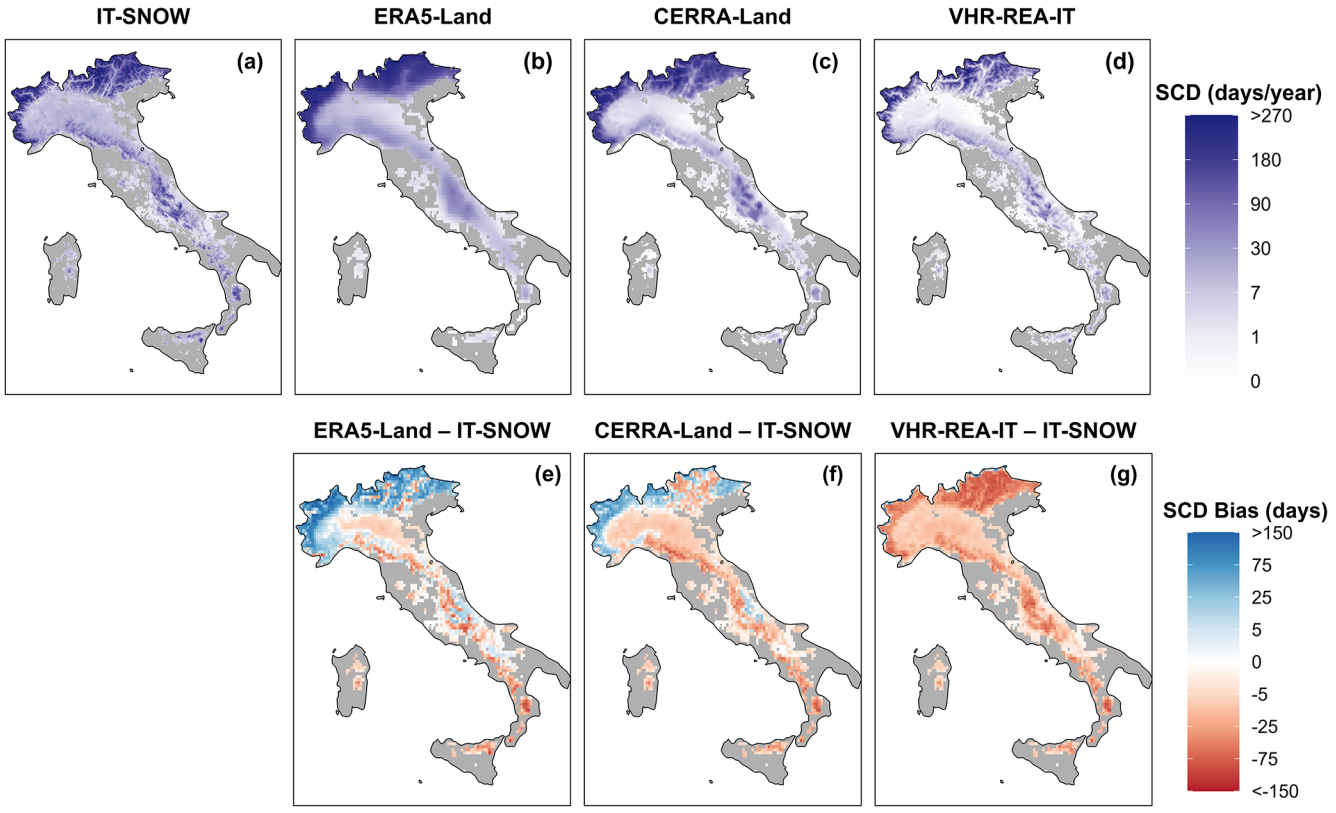


Figure 4. Comparison of mean annual snow cover duration (SCD) for the period September 2010–August 2024. **(a–d)** Mean annual SCD maps for the IT-SNOW reference dataset and the three land-surface products at their native resolutions. **(e–g)** Spatial bias maps (Product – IT-SNOW) showing the difference in SCD in days with common 9 km grid.

mation over the north-western Alps inflates both snow accumulation and snow persistence, and the SCD overestimation confirms that these forcing biases translate into prolonged snow cover seasons. In the Apennines, SCD biases are predominantly negative but vary across subregions. The northern Apennines show the most widespread underestimation, consistent with the autumn and winter precipitation deficits identified for these sectors in Sect. 5.1, which limit the number of days on which SWE is at least 5 mm and thus shorten the simulated snow season. A similarly widespread negative SCD bias is observed across the southern Apennines. The central Apennines display a mixed pattern: negative SCD biases over the higher massifs occur alongside locally positive biases in lower-lying areas, where reference SCD is short and SWE is also slightly overestimated. The drivers of this mixed, elevation-dependent pattern are difficult to isolate. It may stem from the same combination of factors hypothesized in Sect. 5.1 for the mean SWE biases, such as the coarse grid representation of the topography and unresolved local snow processes.

CERRA-Land shows a more moderate Alpine SCD overestimation than ERA5-Land, while maintaining negative biases across the Apennines (Fig. 4, panel f). With the exception of some valleys in the central-eastern Alps, where the product underestimates SCD, most of the Alps show positive SCD bias, with the strongest and most spatially coherent overestimation occurring over the north-western portion of the chain, near the Swiss and French borders. This pattern aligns with the findings of Monteiro and Morin (2023), who reported that CERRA-Land particularly overestimates SCD over the western Italian Alps when compared against MODIS satellite observations. As discussed in Sect. 5.1, positive autumn–winter precipitation biases and colder conditions in this subregion favour both excessive accumulation and prolonged snow retention. Over the most eastern Alps, the positive SCD bias is weaker but still present, consistent with the comparatively modest annual SWE biases in these sectors. Across all three Apennine subregions and southern Italy, CERRA-Land underestimates SCD, with the strongest negative bias in the northern Apennines, consistent with the most severe precipitation deficits in the snow accumulation season identified in Sect. 5.1 (Fig. C2, panels a and b). In the central and southern Apennines, autumn and winter precipitation underestimation likewise coincides with negative SCD biases, whereas positive precipitation biases are concentrated in the warmer seasons and therefore provide little support for snow persistence.

VHR-REA_IT (panel g) underestimates SCD across all subregions in both the Alps and the Apennines. Unlike ERA5-Land and CERRA-Land, which show opposing SCD bias signs between the Alps and the Apennines, VHR-REA_IT is the only product with consistently negative SCD biases across all subregions. Within the Alps, the underestimation intensifies from the north-western sector towards the central and eastern sectors, where the SCD deficit is the largest among all subregions despite winter precipitation overestimation and cold temperature biases (Fig. C3, panels b and f), suggesting that forcing biases alone cannot explain the pattern and that the snow-model structure or parameterisation may have an important role, as discussed for mean annual SWE. Overall, VHR-REA_IT exhibits the poorest SCD performance among the three evaluated products.

5.3 Temporal correlation of daily SWE

To complement the assessment of annual snowpack characteristics, we evaluated how well each product reproduces the day-to-day variability of SWE through temporal correlation analysis. The Pearson correlation coefficient (r) was calculated at each grid cell between the daily SWE time series of each product and of the IT-SNOW reference, for the entire study period (September 2010–August 2024), following resampling to the common ERA5-Land 9 km spatial resolution. The results are presented in Fig. 5, which displays spatial maps of the correlation coefficients, providing a direct visual assessment of temporal correspondence between simulated and reference snowpack dynamics across Italy.

Overall, ERA5-Land demonstrates the highest daily correlations among the three products, with the strongest agreement in the Alpine region and weaker but still comparatively better performance in the Apennines. Despite the substantial overestimation of SWE magnitude at higher elevations documented in Sect. 5.1, the temporal variability of the simulated snowpack remains broadly consistent with the reference, particularly in the Alps. This is consistent with the offline product architecture described in Sect. 3.2.1: as ERA5's atmospheric data assimilation constrains the sequence and timing of synoptic weather events, the forcing inherited by CHTESSEL is expected to preserve realistic temporal patterns even where simulated mean annual SWE and SCD are biased at the land surface. Similar behaviour has been reported in other mountainous regions, where ERA5-Land maintains reasonable temporal consistency with the reference despite substantial magnitude biases: over parts of Iran, ERA5-Land preserves temporal consistency while overestimating snow depth (Majidi et al., 2025), and over parts of Canada it does so while underestimating SWE (Kanda and Fletcher, 2024).

CERRA-Land shows daily correlation patterns broadly comparable to ERA5-Land across the Alpine region, with similar spatial structure and only slightly lower coefficients in the north-western sector. In the Apennines, however, the correlation weakens more substantially than for ERA5-Land, particularly in the northern sector. This stronger degradation is consistent with the more severe autumn and winter precipitation deficits in CERRA-Land's forcing over the Apennines discussed in Sect. 5.1 (Fig. C2, panels a and b), which exceed those of ERA5-Land in the same subregions. In these lower-elevation Apennine regions, where snow cover is more intermittent, such deficits are more likely to reduce the simulated duration and continuity of snow cover during periods when the reference indicates snow presence, thereby affecting not only snow amount but also snow persistence and weakening the temporal correspondence of daily SWE with the reference time series.

VHR-REA_IT exhibits markedly poorer performance in capturing daily SWE dynamics, with substantially lower daily correlations throughout most of Italy, particularly in the Apennines and at lower elevations where correlations fall into the lowest class of the colour scale. This weak temporal correspondence is consistent with VHR-REA_IT's systematic underestimation of both mean annual SWE and SCD documented in Sect. 5.1 and 5.2. The severe underestimation of SWE produces frequent zero or near-zero values when a substantial snowpack should exist, thereby degrading the correlation. Therefore, the model fails to capture day-to-day variability for snow that it incorrectly simulates as absent.

6 Conclusions

This study evaluated SWE estimates from three land-surface products, ERA5-Land, CERRA-Land, and VHR-REA_IT, against the IT-SNOW reference over Italy using three complementary indicators: mean annual SWE, snow cover duration, and temporal correlation of daily SWE series. To support the interpretation of the identified SWE discrepancies, the analysis also incorporated a complementary evaluation of the products' precipitation and temperature biases relative to the gauge-based national reference SCIA fields. The results show that product performance varies across the different Italian mountain regions and different indications may be drawn from the evaluation metrics. The complementary precipitation and temperature analysis helps to attribute a substantial part of the SWE differences to their meteorological origins, although in some regions and products the forcing biases alone do not fully account for the SWE discrepancies (Liu et al., 2022; Fang et al., 2023).

Among the three products, ERA5-Land showed the strongest positive biases in mean annual SWE and snow cover duration in the Alpine domain, especially in the north-western and central Alps, where precipitation overestimation and persistent cold biases favour both excessive accumulation and prolonged snow persistence. In the Apennines, by contrast, ERA5-Land generally underestimated both mean SWE and snow cover duration, consistent with autumn and winter precipitation deficits that limit snow accumulation. Despite these magnitude biases, ERA5-Land achieved the

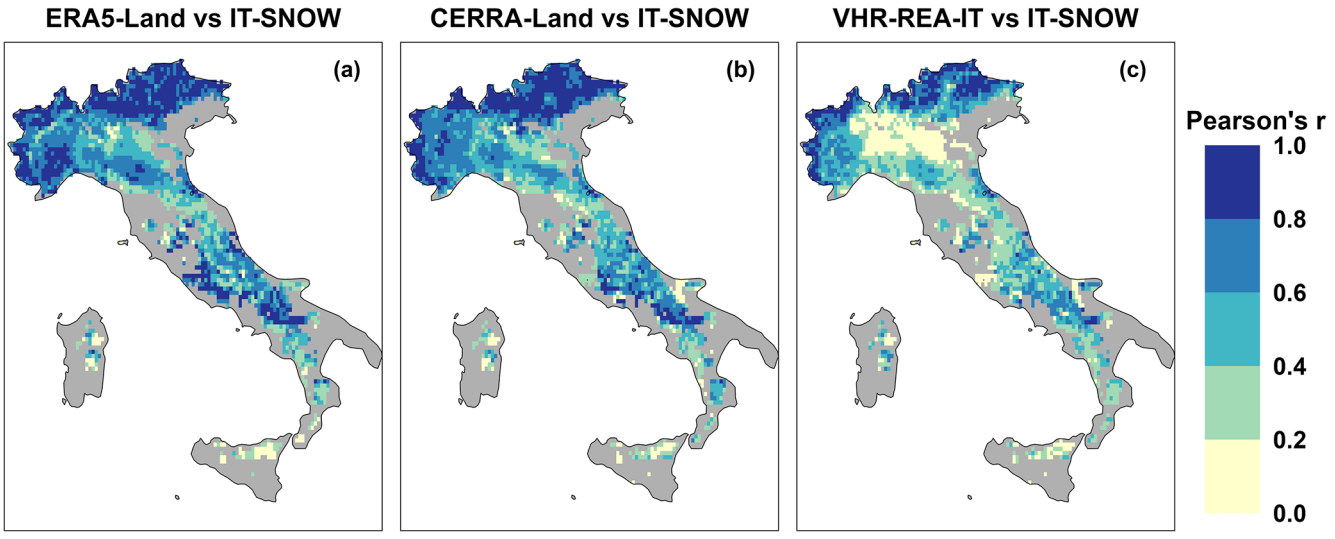


Figure 5. Temporal correlation of daily snow water equivalent (SWE) between each evaluated product and the IT-SNOW reference for the period September 2010–August 2024. The maps display the Pearson correlation coefficient (r) for **(a)** ERA5-Land, **(b)** CERRA-Land, and **(c)** VHR-REA_IT with common grid at 9 km resolution.

strongest temporal correlations with IT-SNOW daily time series, indicating that it reproduces day-to-day snowpack variability more faithfully than the other products. CERRA-Land reproduced spatial SWE patterns in more detail than ERA5-Land due to its finer resolution, but still underestimated mean SWE across most analysed subregions, with the main exception of the north-western Alps. In the central and eastern Alps, CERRA-Land exhibits negative mean annual SWE bias alongside positive SCD bias, suggesting that the snowpack, while smaller in total mass, persists longer than indicated by the reference. This is consistent with the persistent cold bias across the snow season in these subregions, which may delay melt onset and extend the snow-covered period even where accumulation is limited by a weak underestimation of winter precipitation. In the Apennines, CERRA-Land showed broadly negative mean SWE and SCD biases, with the strongest deficits in the northern Apennines. VHR-REA_IT exhibited the poorest overall performance, with the most spatially widespread underestimation of SWE and SCD and the weakest daily correlations. The systematic underestimation of snow mass is the central limitation: by reducing the simulated snowpack, it shortens the snow-covered period and introduces prolonged mismatches with the reference time series, which in turn degrade the temporal correspondence. The results suggest that these limitations are consistent with the absence of observational assimilation within the regional domain: unlike ERA5-Land and CERRA-Land, whose forcing fields inherit observational constraints from their parent atmospheric reanalyses, VHR-REA_IT meteorological fields evolve freely within its boundaries, leaving biases generated during the simulation uncorrected. This is notable given that VHR-REA_IT combines the finest grid spacing with the most complete land–atmosphere coupling among the evaluated products: higher resolution alone does not guarantee more accurate SWE, and the assimilation of meteorological observations remains essential in high-resolution applications. A full understanding of the remaining discrepancies will require dedicated process-level and sensitivity analyses to isolate the respective roles of forcing, snow model structure, and coupled land–atmosphere feedbacks, which are beyond the scope of this work.

A central motivation of this study was to assess whether any of the evaluated products could be reliably used for extending SWE information beyond the relatively short IT-SNOW period. In this respect, ERA5-Land appears to be the most promising candidate, not so much because it provides the most accurate snow magnitudes, but because it shows the highest temporal fidelity across much of the domain. This may support applications focused on interannual variability, anomaly detection, or standardised snow indices, provided that the consistency of bias characteristics over time is carefully assessed, and systematic biases are accounted for, before its use in long-term hydro-climatological analyses. CERRA-Land also shows potential, particularly in parts of the Alpine domain, but its performance over the entirety of Italy appears limited by the quality of precipitation forcing. Given that CERRA-Land precipitation is refined through the MESCAN analysis system, the contrast between the present results and more favourable findings reported elsewhere in Europe (Monteiro and Morin, 2023) suggests that the gauge density of the assimilated precipitation plays an important role in controlling its added value. VHR-REA_IT, in its current form, does not provide a sufficiently reliable basis for record extension, although its convection-permitting reso-

lution and fully coupled architecture represent a physically more ambitious framework than the offline configurations of the other two products; realising this potential would likely require the incorporation of observational constraints within the regional domain.

More broadly, this study shows that evaluating SWE products jointly with the meteorological fields that drive the snow accumulation and melt modelling allows a more comprehensive interpretation of their differences and of the performance indicators, since it helps to distinguish where SWE biases are primarily consistent with forcing errors and where additional factors related to snow process representation are likely involved. This provides a transferable evaluation framework for other regions where benchmark snow datasets are available for a limited period only.

Appendix A: Seasonal and ephemeral snow regimes over the study domain

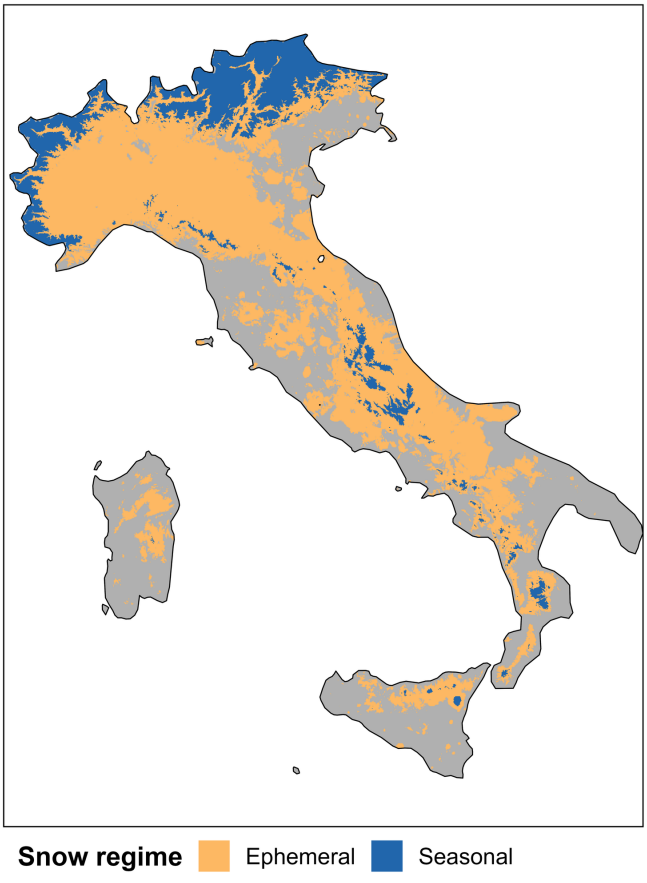


Figure A1. Seasonal and ephemeral snow regimes over the study domain, derived from the IT-SNOW daily SWE series for the period September 2010–August 2024. Grey shading marks the cells outside the analysis domain.

Appendix B: Mean annual precipitation and temperature biases

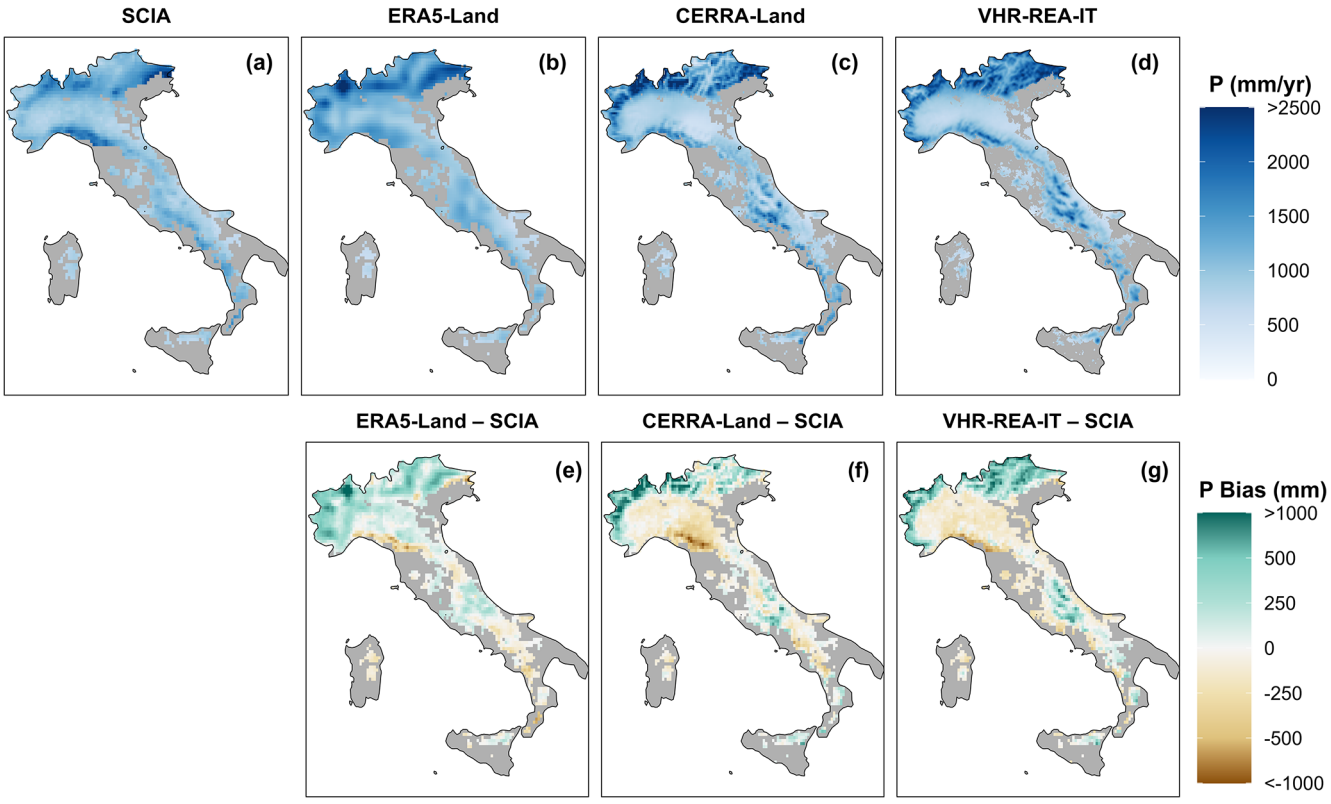


Figure B1. Comparison of mean annual precipitation for the period September 2010–August 2024. **(a–d)** Mean annual precipitation maps for the SCIA reference dataset and the three land-surface products (ERA5-Land, CERRA-Land, VHR-REA_IT) at their native resolutions. **(e–g)** Spatial bias maps (Product – SCIA) showing the difference in precipitation between each of the three land-surface products and the reference dataset, resampled to a common 9 km grid. Positive values indicate overestimation; negative values indicate underestimation.

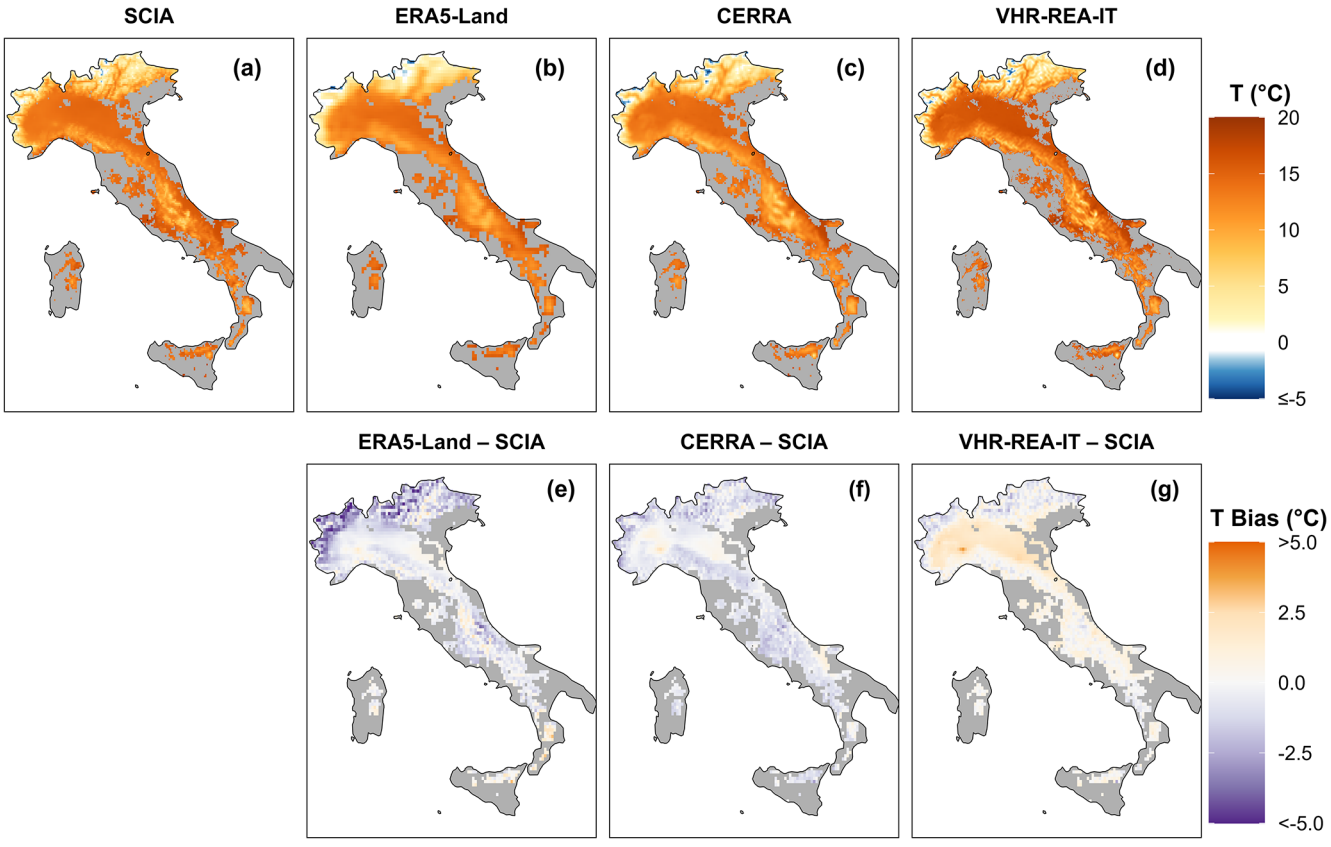


Figure B2. Comparison of mean annual temperature for the period September 2010–August 2024. **(a–d)** Mean annual temperature maps for the SCIA reference dataset and three land-surface products (ERA5-Land, CERRA-Land, VHR-REA_IT) at their native resolutions. **(e–g)** Spatial bias maps (Product – SCIA) showing the difference in temperature between each of the three land-surface products and the reference dataset, resampled to a common 9 km grid. Positive values indicate warm bias; negative values indicate cold bias.

Appendix C: Mean seasonal biases in precipitation, temperature and SWE

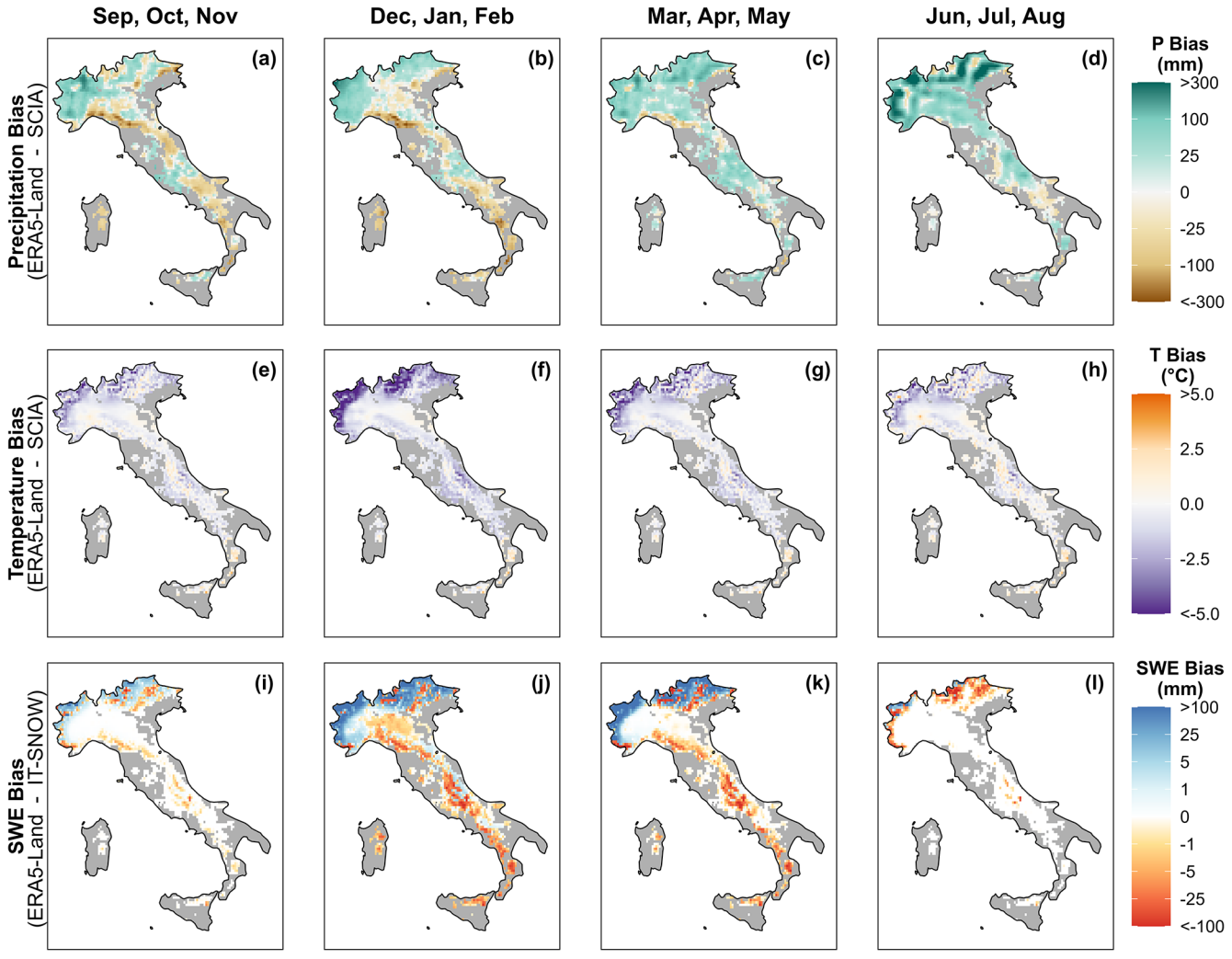


Figure C1. Seasonal biases in precipitation, temperature, and snow water equivalent for ERA5-Land relative to reference datasets (SCIA for precipitation and temperature; IT-SNOW for SWE) for the period September 2010–August 2024. The first row **(a–d)** shows precipitation bias (ERA5-Land – SCIA), the second row **(e–h)** shows temperature bias (ERA5-Land – SCIA), and the third row **(i–l)** shows SWE bias (ERA5-Land – IT-SNOW). Each column represents the calendar season: **(a, e, i)** Autumn (September–November), **(b, f, j)** Winter (December–February), **(c, g, k)** Spring (March–May), and **(d, h, l)** Summer (June–August). All bias maps are resampled to a common 9 km grid. Positive values indicate overestimation by ERA5-Land; negative values indicate underestimation.

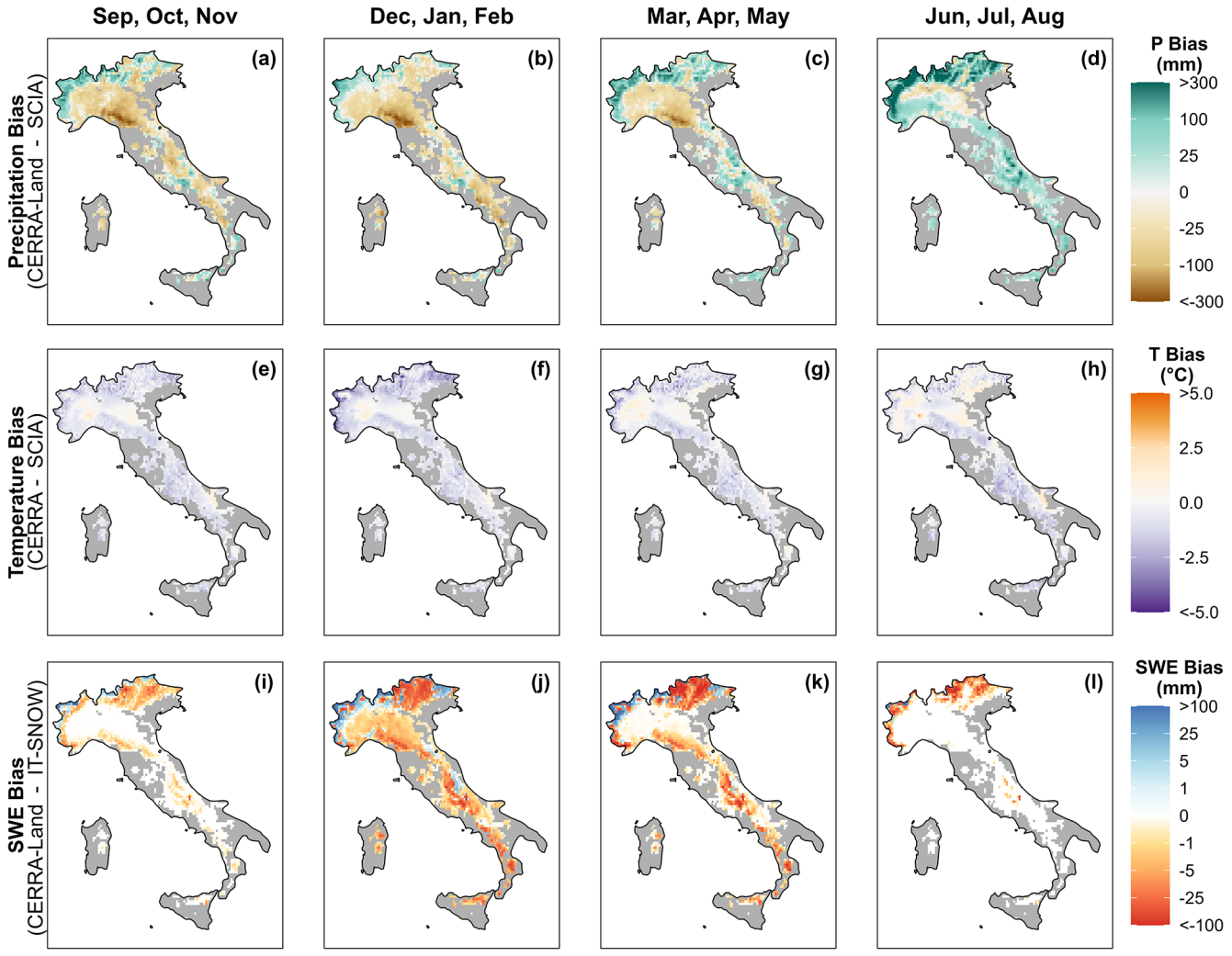


Figure C2. Seasonal biases in precipitation, temperature, and snow water equivalent for CERRA-Land relative to reference datasets (SCIA for precipitation and temperature; IT-SNOW for SWE) for the period September 2010–August 2024. The first row **(a–d)** shows precipitation bias (CERRA-Land – SCIA), the second row **(e–h)** shows temperature bias (CERRA – SCIA), and the third row **(i–l)** shows SWE bias (CERRA-Land – IT-SNOW). Each column represents the calendar season: **(a, e, i)** Autumn (September–November), **(b, f, j)** Winter (December–February), **(c, g, k)** Spring (March–May), and **(d, h, l)** Summer (June–August). All bias maps are resampled to a common 9 km grid. Positive values indicate overestimation by CERRA-Land; negative values indicate underestimation.

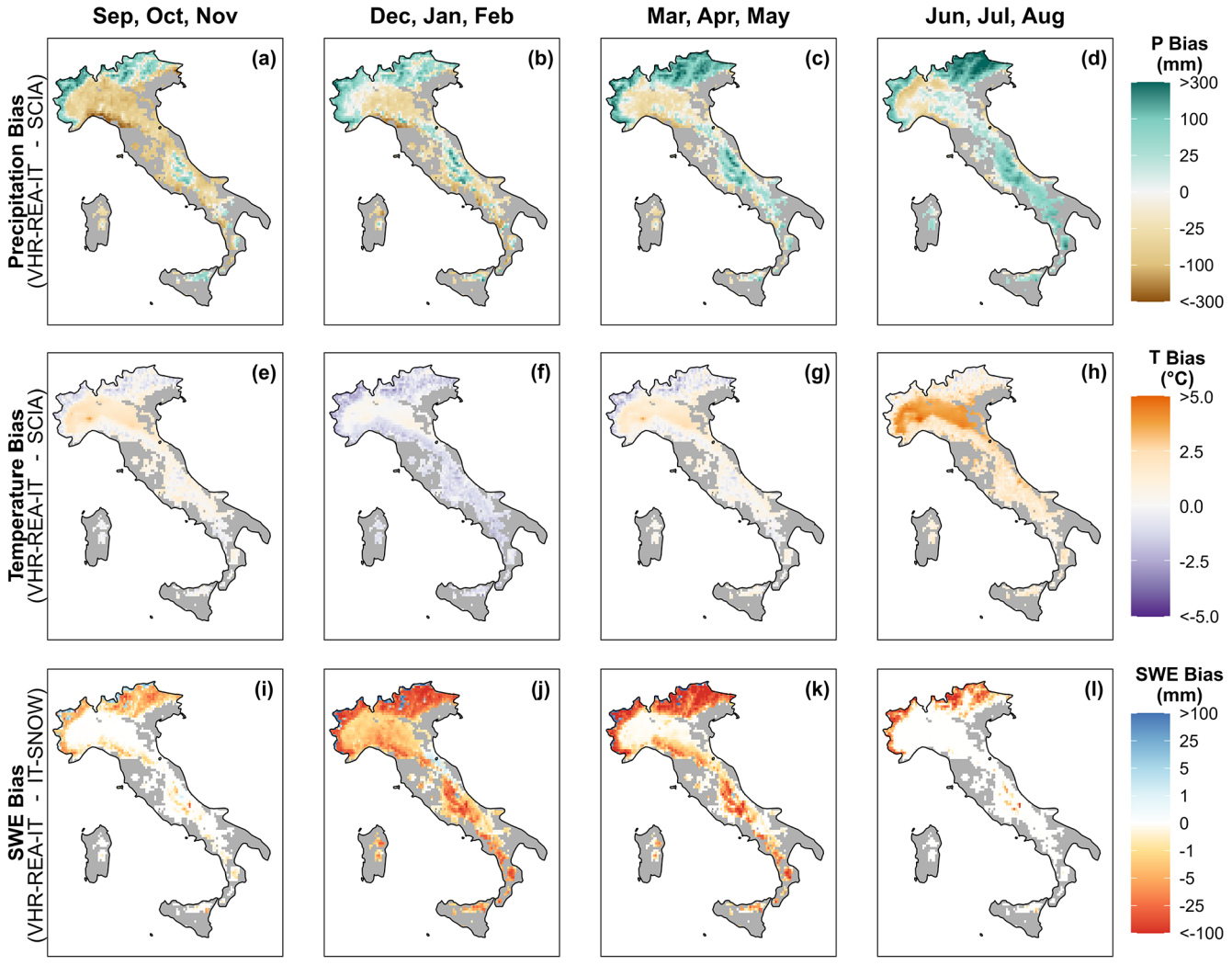


Figure C3. Seasonal biases in precipitation, temperature, and snow water equivalent for VHR-REA_IT relative to reference datasets (SCIA for precipitation and temperature; IT-SNOW for SWE) for the period September 2010–August 2024. The first row **(a–d)** shows precipitation bias (VHR-REA_IT – SCIA), the second row **(e–h)** shows temperature bias (VHR-REA_IT – SCIA), and the third row **(i–l)** shows SWE bias (VHR-REA_IT – IT-SNOW). Each column represents the calendar season: **(a, e, i)** Autumn (September–November), **(b, f, j)** Winter (December–February), **(c, g, k)** Spring (March–May), and **(d, h, l)** Summer (June–August). All bias maps are resampled to a common 9 km grid. Positive values indicate overestimation by VHR-REA_IT; negative values indicate underestimation.

Data availability. All datasets analysed in this study are publicly available. IT-SNOW is available from Zenodo (https://doi.org/10.5281/zenodo.17226478, Avanzi et al., 2025). ERA5-Land and CERRA-Land are available from the Copernicus Climate Change Service Climate Data Store (https://doi.org/10.24381/cds.e2161bac, Copernicus Climate Change Service, 2019, and https://doi.org/10.24381/cds.a7f3cd0b, Copernicus Climate Change Service, 2022, respectively). VHR-REA_IT is available from the CMCC Data Delivery System (https://doi.org/10.25424/cmcc/era5-2km_italy, CMCC, 2021). The SCIA precipitation and temperature data are available from ISPRA (https://scia.isprambiente.it, last access: 27 October 2026).

Supplement. The supplement related to this article is available online at https://doi.org/10.5194/hess-30-6763-2026-supplement.

Author contributions. GS: conceptualization, data curation, formal analysis, investigation, methodology, validation, visualization, writing – original draft, writing – review and editing. MN: conceptualization, investigation, methodology, validation, supervision, writing – review and editing. FA: supervision, writing – review and editing. ET: conceptualization, investigation, methodology, resources, validation, supervision, writing – review and editing.

Competing interests. At least one of the (co-)authors is a member of the editorial board of *Hydrology and Earth System Sciences*. The peer-review process was guided by an independent editor, and the authors also have no other competing interests to declare.

Disclaimer. Publisher's note: Copernicus Publications remains neutral with regard to jurisdictional claims made in the text, published maps, institutional affiliations, or any other geographical representation in this paper. The authors bear the ultimate responsibility for providing appropriate place names. Views expressed in the text are those of the authors and do not necessarily reflect the views of the publisher.

Financial support. This study was carried out within the RETURN Extended Partnership under European Union Next-GenerationEU (National Recovery and Resilience Plan – NRRP, Mission 4, Component 2, Investment 1.3 – D.D. 1243 2/8/2022, PE0000005), and within the project "Stochastic amplification of climate change into floods and droughts change (CO22Water)" – FIS00000846 – CUP J53C23003860001. This publication is funded by the Italian Science Fund under FIS1.

Review statement. This paper was edited by Daniel Viviroli and reviewed by Steven Margulis and one anonymous referee.

References

Adinolfi, M., Raffa, M., Reder, A., and Mercogliano, P.: Investigation on potential and limitations of ERA5 Reanalysis downscaled on Italy by a convection-permitting model, Clim. Dynam., 61, 4319–4342, https://doi.org/10.1007/s00382-023-06803-w, 2023.

AINEVA: Appennini, resoconto stagione 2022–2023, Associazione Interregionale Neve e Valanghe, https://aineva.it/wp-content/uploads/Pubblicazioni/resoconto2022-23/appennini2022-23.pdf (last access: 27 October 2026), 2023.

Avanzi, F., Gabellani, S., Delogu, F., Silvestro, F., Cremonese, E., Morra di Cella, U., Ratto, S., and Stevenin, H.: Snow Multi-data Mapping and Modeling (S3M) 5.1: a distributed cryospheric model with dry and wet snow, data assimilation, glacier mass balance, and debris-driven melt, Geosci. Model Dev., 15, 4853–4879, https://doi.org/10.5194/gmd-15-4853-2022, 2022.

Avanzi, F., Gabellani, S., Delogu, F., Silvestro, F., Pignone, F., Bruno, G., Pulvirenti, L., Squicciarino, G., Fiori, E., Rossi, L., Puca, S., Toniazzo, A., Giordano, P., Falzacappa, M., Ratto, S., Stevenin, H., Cardillo, A., Fioletti, M., Cazzuli, O., Cremonese, E., Morra di Cella, U., and Ferraris, L.: IT-SNOW: a snow reanalysis for Italy blending modeling, in situ data, and satellite observations (2010–2021), Earth Syst. Sci. Data, 15, 639–660, https://doi.org/10.5194/essd-15-639-2023, 2023.

Avanzi, F., Munerol, F., Milelli, M., Gabellani, S., Massari, C., Girotto, M., Cremonese, E., Galvagno, M., Bruno, G., Morra di Cella, U., Rossi, L., Altamura, M., and Ferraris, L.: Winter snow deficit was a harbinger of summer 2022 socio-hydrologic drought in the Po Basin, Italy, Commun. Earth Environ., 5, 64, https://doi.org/10.1038/s43247-024-01222-z, 2024.

Avanzi, F., Gabellani, S., Delogu, F., Silvestro, F., Pignone, F., Bruno, G., Pulvirenti, L., Squicciarino, G., Fiori, E., Rossi, L., Puca, S., Toniazzo, A., Giordano, P., Falzacappa, M., Ratto, S., Stevenin, H., Cardillo, A., Fioletti, M., Cazzuli, O., Cremonese, E., Morra di Cella, U., and Ferraris, L.: IT-SNOW: a snow reanalysis for Italy blending modeling, in-situ data, and satellite observations, Version v5, Zenodo [data set], https://doi.org/10.5281/zenodo.17226478, 2025.

Baatz, R., Hendricks Franssen, H. J., Euskirchen, E., Sihi, D., Dietze, M., Ciavatta, S., Fennel, K., Beck, H., De Lannoy, G., Pauwels, V. R. N., Raiho, A., Montzka, C., Williams, M., Mishra, U., Poppe, C., Zacharias, S., Lausch, A., Samaniego, L., Van Looy, K., Bogena, H., Adamescu, M., Mirtl, M., Fox, A., Goergen, K., Naz, B. S., Zeng, Y., and Vereecken, H.: Reanalysis in Earth System Science: Toward Terrestrial Ecosystem Reanalysis, Rev. Geophys., 59, e2020RG000715, https://doi.org/10.1029/2020RG000715, 2021.

Bales, R. C., Molotch, N. P., Painter, T. H., Dettinger, M. D., Rice, R., and Dozier, J.: Mountain hydrology of the western United States, Water Resour. Res., 42, https://doi.org/10.1029/2005WR004387, 2006.

Balsamo, G., Beljaars, A., Scipal, K., Viterbo, P., Hurk, B. van den, Hirschi, M., and Betts, A. K.: A Revised Hydrology for the ECMWF Model: Verification from Field Site to Terrestrial Water Storage and Impact in the Integrated Forecast System, J. Hydrometeorol., 10, 623–643, https://doi.org/10.1175/2008JHM1068.1, 2009.

Barnett, T. P., Adam, J. C., and Lettenmaier, D. P.: Potential impacts of a warming climate on water avail-

ability in snow-dominated regions, Nature, 438, 303–309, https://doi.org/10.1038/nature04141, 2005.

Bengtsson, L., Andrae, U., Aspelien, T., Batrak, Y., Calvo, J., Rooy, W. de, Gleeson, E., Hansen-Sass, B., Homleid, M., Hortal, M., Ivarsson, K.-I., Lenderink, G., Niemelä, S., Nielsen, K. P., Onvlee, J., Rontu, L., Samuelsson, P., Muñoz, D. S., Subias, A., Tijm, S., Toll, V., Yang, X., and Køltzow, M. Ø.: The HARMONIE–AROME Model Configuration in the ALADIN–HIRLAM NWP System, Mon. Weather Rev., 145, 1919–1935, https://doi.org/10.1175/MWR-D-16-0417.1, 2017.

Benjamini, Y. and Hochberg, Y.: Controlling the False Discovery Rate: A Practical and Powerful Approach to Multiple Testing, J. R. Stat. Soc. B, 57, 289–300, https://doi.org/10.1111/j.2517-6161.1995.tb02031.x, 1995.

Betts, A. K., Ball, J. H., Beljaars, A. C. M., Miller, M. J., and Viterbo, P. A.: The land surface–atmosphere interaction: A review based on observational and global modeling perspectives, J. Geophys. Res.-Atmos., 101, 7209–7225, https://doi.org/10.1029/95JD02135, 1996.

Bocchiola, D. and Diolaiuti, G.: Evidence of climate change within the Adamello Glacier of Italy, Theor. Appl. Climatol., 100, 351–369, https://doi.org/10.1007/s00704-009-0186-x, 2010.

Boone, A. and Etchevers, P.: An Intercomparison of Three Snow Schemes of Varying Complexity Coupled to the Same Land Surface Model: Local-Scale Evaluation at an Alpine Site, J. Hydrometeorol., 2, 374–394, https://doi.org/10.1175/1525-7541(2001)002<0374:AIOTSS>2.0.CO;2, 2001.

Bormann, K., Brown, R., Derksen, C., and Painter, T.: Estimating snow-cover trends from space, Nat. Clim. Change, 8, https://doi.org/10.1038/s41558-018-0318-3, 2018.

Brown, R., Tapsoba, D., and Derksen, C.: Evaluation of snow water equivalent datasets over the Saint-Maurice river basin region of southern Québec, Hydrol. Process., 32, 2748–2764, https://doi.org/10.1002/hyp.13221, 2018.

Broxton, P. D., Zeng, X., and Dawson, N.: Why Do Global Reanalyses and Land Data Assimilation Products Underestimate Snow Water Equivalent?, J. Hydrometeorol., 17, 2743–2761, https://doi.org/10.1175/jhm-d-16-0056.1, 2016.

Bruno, G., Pignone, F., Silvestro, F., Gabellani, S., Schiavi, F., Rebora, N., Giordano, P., and Falzacappa, M.: Performing Hydrological Monitoring at a National Scale by Exploiting Rain-Gauge and Radar Networks: The Italian Case, Atmosphere, 12, 771, https://doi.org/10.3390/atmos12060771, 2021.

Cavalleri, F., Viterbo, F., Brunetti, M., Bonanno, R., Manara, V., Lussana, C., Lacavalla, M., and Maugeri, M.: Inter-comparison and validation of high-resolution surface air temperature reanalysis fields over Italy, Int. J. Climatol., 44, 2681–2700, https://doi.org/10.1002/joc.8475, 2024a.

Cavalleri, F., Lussana, C., Viterbo, F., Brunetti, M., Bonanno, R., Manara, V., Lacavalla, M., Sperati, S., Raffa, M., Capecchi, V., Cesari, D., Giordani, A., Cerenzia, I. M. L., and Maugeri, M.: Multi-scale assessment of high-resolution reanalysis precipitation fields over Italy, Atmos. Res., 312, 107734, https://doi.org/10.1016/j.atmosres.2024.107734, 2024b.

CMCC: ERA5 downscaling @2.2 km over Italy, CMCC Data Delivery System [data set], https://doi.org/10.25424/cmcc/era5-2km_italy, 2021.

Chang, A. T. C., Foster, J. L., and Hall, D. K.: Nimbus-7 SMMR Derived Global Snow Cover Parameters, Ann. Glaciol., 9, 39–44, https://doi.org/10.3189/S0260305500200736, 1987.

Cho, E., Vuyovich, C. M., Kumar, S. V., Wrzesien, M. L., Kim, R. S., and Jacobs, J. M.: Precipitation biases and snow physics limitations drive the uncertainties in macroscale modeled snow water equivalent, Hydrol. Earth Syst. Sci., 26, 5721–5735, https://doi.org/10.5194/hess-26-5721-2022, 2022.

Copernicus Climate Change Service: ERA5-Land hourly data from 1950 to present, Copernicus Climate Change Service (C3S) Climate Data Store (CDS) [data set], https://doi.org/10.24381/cds.e2161bac, 2019.

Copernicus Climate Change Service: CERRA-Land sub-daily regional reanalysis data for Europe from 1984 to present, ECMWF [data set], https://doi.org/10.24381/cds.a7f3cd0b, 2022.

Cortés, G. and Margulis, S.: Impacts of El Niño and La Niña on interannual snow accumulation in the Andes: Results from a high-resolution 31 year reanalysis, Geophys. Res. Lett., 44, 6859–6867, https://doi.org/10.1002/2017GL073826, 2017.

Courtier, P., Thépaut, J.-N., and Hollingsworth, A.: A strategy for operational implementation of 4D-Var, using an incremental approach, Q. J. Roy. Meteor. Soc., 120, 1367–1387, https://doi.org/10.1002/qj.49712051912, 1994.

Dalla Torre, D., Di Marco, N., Menapace, A., Avesani, D., Righetti, M., and Majone, B.: Suitability of ERA5-Land reanalysis dataset for hydrological modelling in the Alpine region, J. Hydrol.: Regional Studies, 52, 101718, https://doi.org/10.1016/j.ejrh.2024.101718, 2024.

Dall'Amico, M., Tasin, S., Di Paolo, F., Brian, M., Leoni, P., Tornatore, F., Formetta, G., Wani, J. M., Rigon, R., and Roati, G.: 30 years (1991–2021) Snow Water Equivalent Dataset in the Po River District, Italy, Sci. Data, 12, 374, https://doi.org/10.1038/s41597-025-04633-5, 2025.

Dawson, N., Broxton, P., and Zeng, X.: Evaluation of Remotely Sensed Snow Water Equivalent and Snow Cover Extent over the Contiguous United States, J. Hydrometeorol., 19, 1777–1791, https://doi.org/10.1175/JHM-D-18-0007.1, 2018.

De Bellis, A., Pavan, V., and Levizzani, V.: Climatologia e variabilità interannuale della neve sull'Appennino Emiliano-Romagnolo, Quaderno Tecnico ARPA-SIMC n. 19/2010, ARPA Emilia-Romagna, Bologna, https://doi.org/10.13140/2.1.4685.7287, 2010.

Decharme, B., Brun, E., Boone, A., Delire, C., Le Moigne, P., and Morin, S.: Impacts of snow and organic soils parameterization on northern Eurasian soil temperature profiles simulated by the ISBA land surface model, The Cryosphere, 10, 853–877, https://doi.org/10.5194/tc-10-853-2016, 2016.

Desiato, F., Lena, F., and Toreti, A.: SCIA: a system for a better knowledge of the Italian climate, B. Geofis. Teor. Appl., 48, 351–358, 2007.

Desiato, F., Fioravanti, G., Fraschetti, P., Perconti, W., and Toreti, A.: Climate indicators for Italy: calculation and dissemination, Adv. Sci. Res., 6, 147–150, https://doi.org/10.5194/asr-6-147-2011, 2011.

Di Marco, N., Avesani, D., Righetti, M., Zaramella, M., Majone, B., and Borga, M.: Reducing hydrological modelling uncertainty by using MODIS snow cover data and a topography-based distribution function snowmelt model, J. Hydrol., 599, 126020, https://doi.org/10.1016/j.jhydrol.2021.126020, 2021.

Doms, G., Förstner, J., Heise, E., Herzog, H.-J., Mironov, D., Raschendorfer, M., Reinhardt, T., Ritter, B., Schrodin, R., Schulz, J.-P., and Vogel, G.: A Description of the Nonhydrostatic Regional COSMO Model, Part II: Physical Parameterization, LM F90 4.20, Consortium for Small-Scale Modelling, Deutscher Wetterdienst, Offenbach, Germany, 161 pp., https://www.cosmo-model.org/content/model/cosmo/coreDocumentation/cosmo_physics_4.20.pdf (last access: 27 October 2026), 2011.

Dong, J., Walker, J. P., and Houser, P. R.: Factors affecting remotely sensed snow water equivalent uncertainty, Remote Sens. Environ., 97, 68–82, https://doi.org/10.1016/j.rse.2005.04.010, 2005.

Dutra, E., Balsamo, G., Viterbo, P., Miranda, P. M. A., Beljaars, A., Schär, C., and Elder, K.: An improved snow scheme for the ECMWF land surface model: Description and offline validation, J. Hydrometeorol., 11, 899–916, https://doi.org/10.1175/2010JHM1249.1, 2010.

Fang, Y., Liu, Y., and Margulis, S. A.: A western United States snow reanalysis dataset over the Landsat era from water years 1985–2021, Sci. Data, 9, 677, https://doi.org/10.1038/s41597-022-01768-7, 2022.

Fang, Y., Liu, Y., Li, D., Sun, H., and Margulis, S. A.: Spatiotemporal snow water storage uncertainty in the midlatitude American Cordillera, The Cryosphere, 17, 5175–5195, https://doi.org/10.5194/tc-17-5175-2023, 2023.

Frei, C. and Schär, C.: A precipitation climatology of the Alps from high-resolution rain-gauge observations, Int. J. Climatol., 18, 873–900, https://doi.org/10.1002/(SICI)1097-0088(19980630)18:8<873::AID-JOC255>3.0.CO;2-9, 1998.

Froidurot, S., Zin, I., Hingray, B., and Gautheron, A.: Sensitivity of Precipitation Phase over the Swiss Alps to Different Meteorological Variables, J. Hydrometeorol., 15, 685–696, https://doi.org/10.1175/JHM-D-13-073.1, 2014.

Froidurot, S., Zin, I., Hingray, B., and Gautheron, A.: Sensitivity of Precipitation Phase over the Swiss Alps to Different Meteorological Variables, J. Hydrometeorol., 15, 685–696, https://doi.org/10.1175/JHM-D-13-073.1, 2014.

Giorgi, F. and Mearns, L. O.: Introduction to special section: Regional climate modeling revisited, J. Geophys. Res.-Atmos., 104, 6335–6352, https://doi.org/10.1029/98JD02072, 1999.

Günther, D., Hanzer, F., Warscher, M., Essery, R., and Strasser, U.: Including Parameter Uncertainty in an Intercomparison of Physically-Based Snow Models, Front. Earth Sci., 8, https://doi.org/10.3389/feart.2020.542599, 2020.

Hall, D. K., Riggs, G. A., Salomonson, V. V., DiGirolamo, N. E., and Bayr, K. J.: MODIS snow-cover products, Remote Sens. Environ., 83, 181–194, https://doi.org/10.1016/S0034-4257(02)00095-0, 2002.

Hersbach, H., Bell, B., Berrisford, P., Hirahara, S., Horányi, A., Muñoz-Sabater, J., Nicolas, J., Peubey, C., Radu, R., Schepers, D., Simmons, A., Soci, C., Abdalla, S., Abellan, X., Balsamo, G., Bechtold, P., Biavati, G., Bidlot, J., Bonavita, M., De Chiara, G., Dahlgren, P., Dee, D., Diamantakis, M., Dragani, R., Flemming, J., Forbes, R., Fuentes, M., Geer, A., Haimberger, L., Healy, S., Hogan, R. J., Hólm, E., Janisková, M., Keeley, S., Laloyaux, P., Lopez, P., Lupu, C., Radnoti, G., de Rosnay, P., Rozum, I., Vamborg, F., Villaume, S., and Thépaut, J.-N.: The ERA5 global reanalysis, Q. J. Roy. Meteor. Soc., 146, 1999–2049, https://doi.org/10.1002/qj.3803, 2020.

Immerzeel, W. W., Lutz, A. F., Andrade, M., Bahl, A., Biemans, H., Bolch, T., Hyde, S., Brumby, S., Davies, B. J., Elmore, A. C., Emmer, A., Feng, M., Fernández, A., Haritashya, U., Kargel, J. S., Koppes, M., Kraaijenbrink, P. D. A., Kulkarni, A. V., Mayewski, P. A., Nepal, S., Pacheco, P., Painter, T. H., Pellicciotti, F., Rajaram, H., Rupper, S., Sinisalo, A., Shrestha, A. B., Viviroli, D., Wada, Y., Xiao, C., Yao, T., and Baillie, J. E. M.: Importance and vulnerability of the world's water towers, Nature, 577, 364–369, https://doi.org/10.1038/s41586-019-1822-y, 2020.

Jenicek, M., Hnilica, J., Nedelcev, O., and Sipek, V.: Future changes in snowpack will impact seasonal runoff and low flows in Czechia, Journal of Hydrology: Regional Studies, 37, 100899, https://doi.org/10.1016/j.ejrh.2021.100899, 2021.

Jones, P. W.: First- and Second-Order Conservative Remapping Schemes for Grids in Spherical Coordinates, Mon. Weather Rev., 127, 2204–2210, https://doi.org/10.1175/1520-0493(1999)127<2204:FASOCR>2.0.CO;2, 1999.

von Kaenel, M. and Margulis, S. A.: Improved modelling of mountain snowpacks with spatially distributed precipitation bias correction derived from historical reanalysis, The Cryosphere, 19, 3309–3327, https://doi.org/10.5194/tc-19-3309-2025, 2025.

Kalnay, E.: Atmospheric Modeling, Data Assimilation and Predictability, Cambridge University Press, 364 pp., https://doi.org/10.1017/CBO9780511802270, 2003.

Kanda, N. and Fletcher, C. G.: Evaluating a hierarchy of bias correction methods for ERA5-Land SWE in northern Canada, EGUsphere [preprint], https://doi.org/10.5194/egusphere-2024-639, 2024.

Kelly, R.: The AMSR-E snow depth algorithm: Description and initial results, Journal of the Remote Sensing Society of Japan, 29, 307–317, https://doi.org/10.11440/rssj.29.307, 2009.

King, F., Erler, A. R., Frey, S. K., and Fletcher, C. G.: Application of machine learning techniques for regional bias correction of snow water equivalent estimates in Ontario, Canada, Hydrol. Earth Syst. Sci., 24, 4887–4902, https://doi.org/10.5194/hess-24-4887-2020, 2020.

Kouki, K., Luojus, K., and Riihelä, A.: Evaluation of snow cover properties in ERA5 and ERA5-Land with several satellite-based datasets in the Northern Hemisphere in spring 1982–2018, The Cryosphere, 17, 5007–5026, https://doi.org/10.5194/tc-17-5007-2023, 2023.

Laprise, R., de Elía, R., Caya, D., Biner, S., Lucas-Picher, P., Diaconescu, E., Leduc, M., Alexandru, A., Separovic, L., and Canadian Network for Regional Climate Modelling and Diagnostics: Challenging some tenets of regional climate modelling, Meteorol. Atmos. Phys., 100, 3–22, https://doi.org/10.1007/s00703-008-0292-9, 2008.

Lievens, H., Demuzere, M., Marshall, H.-P., Reichle, R. H., Brucker, L., Brangers, I., De Rosnay, P., Dumont, M., Girotto, M., Immerzeel, W. W., Jonas, T., Kim, E. J., Koch, I., Marty, C., Saloranta, T., Schöber, J., and De Lannoy, G. J. M.: Snow depth variability in the Northern Hemisphere mountains observed from space, Nat. Commun., 10, https://doi.org/10.1038/s41467-019-12566-y, 2019.

Lindsay, R., Wensnahan, M., Schweiger, A., and Zhang, J.: Evaluation of Seven Different Atmospheric Reanalysis Products in the Arctic, J. Climate, 27, 2588–2606, https://doi.org/10.1175/JCLI-D-13-00014.1, 2014.

Liu, Y., Fang, Y., and Margulis, S. A.: Spatiotemporal distribution of seasonal snow water equivalent in High Mountain Asia from an 18 year Landsat – MODIS era snow reanalysis dataset, The Cryosphere, 15, 5261–5280, https://doi.org/10.5194/tc-15-5261-2021, 2021.

Liu, Y., Fang, Y., Li, D., and Margulis, S. A.: How well do global snow products characterize snow storage in High Mountain Asia?, Geophys. Res. Lett., 49, e2022GL100082, https://doi.org/10.1029/2022GL100082, 2022.

Loprieno, L., Raffa, M., Campanale, A., and Mercogliano, P.: VHR-REA_IT: Transitioning from COSMO-CLM to ICON-CLM at convection-permitting scales, CMCC Technical Note TN0300, Fondazione CMCC Centro Euro-Mediterraneo sui Cambiamenti Climatici, Lecce, Italy, https://files.cmcc.it/Technical_notes/TN0300-remhi-10-2024.pdf (last access: 27 October 2026), 2024.

Main-Knorn, M., Pflug, B., Louis, J., Debaecker, V., Müller-Wilm, U., and Gascon, F.: Sen2Cor for Sentinel-2, in: Image and Signal Processing for Remote Sensing XXIII, P. Soc. Photo-Opt. Ins., XXIII, 37–48, https://doi.org/10.1117/12.2278218, 2017.

Majidi, F., Sabetghadam, S., Gharaylou, M., and Rezaian, R.: Evaluation of the performance of ERA5, ERA5-Land and MERRA-2 reanalysis to estimate snow depth over a mountainous semi-arid region in Iran, J. Hydrol.: Regional Studies, 58, 102246, https://doi.org/10.1016/j.ejrh.2025.102246, 2025.

Masson, V., Le Moigne, P., Martin, E., Faroux, S., Alias, A., Alkama, R., Belamari, S., Barbu, A., Boone, A., Bouyssel, F., Brousseau, P., Brun, E., Calvet, J.-C., Carrer, D., Decharme, B., Delire, C., Donier, S., Essaouini, K., Gibelin, A.-L., Giordani, H., Habets, F., Jidane, M., Kerdraon, G., Kourzeneva, E., Lafaysse, M., Lafont, S., Lebeaupin Brossier, C., Lemonsu, A., Mahfouf, J.-F., Marguinaud, P., Mokhtari, M., Morin, S., Pigeon, G., Salgado, R., Seity, Y., Taillefer, F., Tanguy, G., Tulet, P., Vincendon, B., Vionnet, V., and Voldoire, A.: The SURFEXv7.2 land and ocean surface platform for coupled or offline simulation of earth surface variables and fluxes, Geosci. Model Dev., 6, 929–960, https://doi.org/10.5194/gmd-6-929-2013, 2013.

Matiu, M. and Hanzer, F.: Bias adjustment and downscaling of snow cover fraction projections from regional climate models using remote sensing for the European Alps, Hydrol. Earth Syst. Sci., 26, 3037–3054, https://doi.org/10.5194/hess-26-3037-2022, 2022.

Matiu, M., Crespi, A., Bertoldi, G., Carmagnola, C. M., Marty, C., Morin, S., Schöner, W., Cat Berro, D., Chiogna, G., De Gregorio, L., Kotlarski, S., Majone, B., Resch, G., Terzago, S., Valt, M., Beozzo, W., Cianfarra, P., Gouttevin, I., Marcolini, G., Notarnicola, C., Petitta, M., Scherrer, S. C., Strasser, U., Winkler, M., Zebisch, M., Cicogna, A., Cremonini, R., Debernardi, A., Faletto, M., Gaddo, M., Giovannini, L., Mercalli, L., Soubeyroux, J.-M., Sušnik, A., Trenti, A., Urbani, S., and Weilguni, V.: Observed snow depth trends in the European Alps: 1971 to 2019, The Cryosphere, 15, 1343–1382, https://doi.org/10.5194/tc-15-1343-2021, 2021.

Mätzler, C.: Applications of the interaction of microwaves with the natural snow cover, Remote Sensing Reviews, 2, 259–387, https://doi.org/10.1080/02757258709532086, 1987.

Miglietta, M. M. and Davolio, S.: Dynamical forcings in heavy precipitation events over Italy: lessons from the HyMeX SOP1 campaign, Hydrol. Earth Syst. Sci., 26, 627–646, https://doi.org/10.5194/hess-26-627-2022, 2022.

Mirza, B. N., Small, E. E., and Raleigh, M. S.: Evaluating the utility of Sentinel-1 in a Data Assimilation System for estimating snow depth in a mountainous basin, The Cryosphere, 19, 6691–6709, https://doi.org/10.5194/tc-19-6691-2025, 2025.

Mizukami, N. and Perica, S.: Spatiotemporal Characteristics of Snowpack Density in the Mountainous Regions of the Western United States, J. Hydrometeorol., 9, 1416–1426, https://doi.org/10.1175/2008JHM981.1, 2008.

Moccia, B., Buonora, L., Bertini, C., Ridolfi, E., Russo, F., and Napolitano, F.: What is our pick? Assessment of satellite and reanalysis precipitation datasets over Italy, J. Hydrol.: Regional Studies, 60, 102487, https://doi.org/10.1016/j.ejrh.2025.102487, 2025.

Montanari, A., Nguyen, H., Rubinetti, S., Ceola, S., Galelli, S., Rubino, A., and Zanchettin, D.: Why the 2022 Po River drought is the worst in the past two centuries, Sci. Adv., 9, eadg8304, https://doi.org/10.1126/sciadv.adg8304, 2023.

Monteiro, D. and Morin, S.: Multi-decadal analysis of past winter temperature, precipitation and snow cover data in the European Alps from reanalyses, climate models and observational datasets, The Cryosphere, 17, 3617–3660, https://doi.org/10.5194/tc-17-3617-2023, 2023.

Mott, R., Winstral, A., Cluzet, B., Helbig, N., Magnusson, J., Mazzotti, G., Quéno, L., Schirmer, M., Webster, C., and Jonas, T.: Operational snow-hydrological modeling for Switzerland, Front. Earth Sci., 11, https://doi.org/10.3389/feart.2023.1228158, 2023.

Mudryk, L., Mortimer, C., Derksen, C., Elias Chereque, A., and Kushner, P.: Benchmarking of snow water equivalent (SWE) products based on outcomes of the SnowPEx+ Intercomparison Project, The Cryosphere, 19, 201–218, https://doi.org/10.5194/tc-19-201-2025, 2025.

Muñoz-Sabater, J., Dutra, E., Agustí-Panareda, A., Albergel, C., Arduini, G., Balsamo, G., Boussetta, S., Choulga, M., Harrigan, S., Hersbach, H., Martens, B., Miralles, D. G., Piles, M., Rodríguez-Fernández, N. J., Zsoter, E., Buontempo, C., and Thépaut, J.-N.: ERA5-Land: a state-of-the-art global reanalysis dataset for land applications, Earth Syst. Sci. Data, 13, 4349–4383, https://doi.org/10.5194/essd-13-4349-2021, 2021.

NOHRSC (National Operational Hydrologic Remote Sensing Center): Snow Data Assimilation System (SNODAS) Data Products at NSIDC, Version 1, National Snow and Ice Data Center (NSIDC), Boulder, Colorado, USA, https://doi.org/10.7265/N5TB14TC, 2004.

Orsolini, Y., Wegmann, M., Dutra, E., Liu, B., Balsamo, G., Yang, K., de Rosnay, P., Zhu, C., Wang, W., Senan, R., and Arduini, G.: Evaluation of snow depth and snow cover over the Tibetan Plateau in global reanalyses using in situ and satellite remote sensing observations, The Cryosphere, 13, 2221–2239, https://doi.org/10.5194/tc-13-2221-2019, 2019.

Pellicciotti, F., Brock, B., Strasser, U., Burlando, P., Funk, M., and Corripio, J.: An enhanced temperature-index glacier melt model including the shortwave radiation balance: development and testing for Haut Glacier d'Arolla, Switzerland, J. Glaciol., 51, 573–587, https://doi.org/10.3189/172756505781829124, 2005.

Petersky, R. and Harpold, A.: Now you see it, now you don't: a case study of ephemeral snowpacks and soil moisture response in the Great Basin, USA, Hydrol. Earth Syst. Sci., 22, 4891–4906, https://doi.org/10.5194/hess-22-4891-2018, 2018.

Pfeffer, W. T., Arendt, A. A., Bliss, A., Bolch, T., Cogley, J. G., Gardner, A. S., Hagen, J.-O., Hock, R., Kaser, G., Kienholz, C., Miles, E. S., Moholdt, G., Mölg, N., Paul, F., Radić, V., Rastner, P., Raup, B. H., Rich, J., Sharp, M. J., and The Randolph Consortium: The Randolph Glacier Inventory: a globally complete inventory of glaciers, J. Glaciol., 60, 537–552, https://doi.org/10.3189/2014JoG13J176, 2014.

Pflug, J. M., Kumar, S. V., Livneh, B., Gutmann, E. D., Gangrade, S., and Kao, S. C.: Comparisons of montane snow water equivalent projections: calculating total snow mass in regions with projection agreement and divergence in the western United States, J. Climate, 38, 855–874, https://doi.org/10.1175/JCLI-D-24-0128.1, 2025.

Pimentel, R., Herrero, J., and Polo, M. J.: Subgrid parameterization of snow distribution at a Mediterranean site using terrestrial photography, Hydrol. Earth Syst. Sci., 21, 805–820, https://doi.org/10.5194/hess-21-805-2017, 2017.

Raffa, M., Reder, A., Marras, G. F., Mancini, M., Scipione, G., Santini, M., and Mercogliano, P.: VHR-REA_IT Dataset: Very High Resolution Dynamical Downscaling of ERA5 Reanalysis over Italy by COSMO-CLM, Data, 6, 88, https://doi.org/10.3390/data6080088, 2021.

Rajulapati, C. R., Papalexiou, S. M., Clark, M. P., Razavi, S., Tang, G., and Pomeroy, J. W.: Assessment of Extremes in Global Precipitation Products: How Reliable Are They?, J. Hydrometeorol., 21, 2855–2873, https://doi.org/10.1175/JHM-D-20-0040.1, 2020.

Raleigh, M. S., Lundquist, J. D., and Clark, M. P.: Exploring the impact of forcing error characteristics on physically based snow simulations within a global sensitivity analysis framework, Hydrol. Earth Syst. Sci., 19, 3153–3179, https://doi.org/10.5194/hess-19-3153-2015, 2015.

Ridal, M., Bazile, E., Le Moigne, P., Randriamampianina, R., Schimanke, S., Andrae, U., Berggren, L., Brousseau, P., Dahlgren, P., Edvinsson, L., El-Said, A., Glinton, M., Hagelin, S., Hopsch, S., Isaksson, L., Medeiros, P., Olsson, E., Unden, P., and Wang, Z. Q.: CERRA, the Copernicus European Regional Reanalysis system, Q. J. Roy. Meteor. Soc., 150, 3385–3411, https://doi.org/10.1002/qj.4764, 2024.

Rockel, B., Will, A., and Hense, A.: The Regional Climate Model COSMO-CLM (CCLM), metz, 17, 347–348, https://doi.org/10.1127/0941-2948/2008/0309, 2008.

Sabetghadam, S., Fletcher, C. G., and Erler, A.: The importance of model horizontal resolution for improved estimation of snow water equivalent in a mountainous region of western Canada, Hydrol. Earth Syst. Sci., 29, 887–902, https://doi.org/10.5194/hess-29-887-2025, 2025.

Santanello, J. A., Dirmeyer, P. A., Ferguson, C. R., Findell, K. L., Tawfik, A. B., Berg, A., Ek, M., Gentine, P., Guillod, B. P., Heerwaarden, C. van, Roundy, J., and Wulfmeyer, V.: Land–Atmosphere Interactions: The LoCo Perspective, B. Am. Meteorol. Soc., 99, 1253–1272, https://doi.org/10.1175/BAMS-D-17-0001.1, 2018.

Sarigil, G., Neri, M., and Toth, E.: Evaluation of national and international gridded meteorological products for rainfall–runoff modelling in Northern Italy, Journal of Hydrology: Regional Studies, 56, 102031, https://doi.org/10.1016/j.ejrh.2024.102031, 2024.

Schrodin, R. and Heise, E.: The Multi-Layer Version of the DWD Soil Model TERRA_LM, COSMO Technical Report No. 2, Deutscher Wetterdienst, Offenbach, Germany, 16 pp., https://doi.org/10.5676/DWD_pub/nwv/cosmo-tr_2, 2001.

Soci, C., Bazile, E., Besson, F., and Landelius, T.: High-resolution precipitation re-analysis system for climatological purposes, Tellus A, 68, 29879, https://doi.org/10.3402/tellusa.v68.29879, 2016.

Soci, C., Hersbach, H., Simmons, A., Poli, P., Bell, B., Berrisford, P., Horányi, A., Muñoz-Sabater, J., Nicolas, J., Radu, R., Schepers, D., Villaume, S., Haimberger, L., Woollen, J., Buontempo, C., and Thépaut, J.-N.: The ERA5 global reanalysis from 1940–2022, Q. J. Roy. Meteor. Soc., 150, 4014–4048, https://doi.org/10.1002/qj.4803, 2024.

Sturm, M., Holmgren, J., and Liston, G. E.: A Seasonal Snow Cover Classification System for Local to Global Applications, J. Climate, 8, 1261–1283, https://doi.org/10.1175/1520-0442(1995)008<1261:ASSCCS>2.0.CO;2, 1995.

Takala, M., Luojus, K., Pulliainen, J., Derksen, C., Lemmetyinen, J., Kärnä, J.-P., Koskinen, J., and Bojkov, B.: Estimating northern hemisphere snow water equivalent for climate research through assimilation of space-borne radiometer data and ground-based measurements, Remote Sens. Environ., 115, 3517–3529, https://doi.org/10.1016/j.rse.2011.08.014, 2011.

Terzago, S., Andreoli, V., Arduini, G., Balsamo, G., Campo, L., Cassardo, C., Cremonese, E., Dolia, D., Gabellani, S., von Hardenberg, J., Morra di Cella, U., Palazzi, E., Piazzi, G., Pogliotti, P., and Provenzale, A.: Sensitivity of snow models to the accuracy of meteorological forcings in mountain environments, Hydrol. Earth Syst. Sci., 24, 4061–4090, https://doi.org/10.5194/hess-24-4061-2020, 2020.

Urraca, R. and Gobron, N.: Temporal stability of long-term satellite and reanalysis products to monitor snow cover trends, The Cryosphere, 17, 1023–1052, https://doi.org/10.5194/tc-17-1023-2023, 2023.

Wilks, D. S.: "The Stippling Shows Statistically Significant Grid Points": How Research Results are Routinely Overstated and Overinterpreted, and What to Do about It, B. Am. Meteorol. Soc., 97, 2263–2273, https://doi.org/10.1175/BAMS-D-15-00267.1, 2016.

Verrelle, A., Michael, G., Eric, B., and Moigne, P. L.: Strengths and weaknesses of the new CERRA-Land surface reanalysis at 5.5 km resolution over Europe, Copernicus Meetings, https://doi.org/10.5194/ems2022-279, 2022.

Vionnet, V., Brun, E., Morin, S., Boone, A., Faroux, S., Le Moigne, P., Martin, E., and Willemet, J.-M.: The detailed snowpack scheme Crocus and its implementation in SURFEX v7.2, Geosci. Model Dev., 5, 773–791, https://doi.org/10.5194/gmd-5-773-2012, 2012.

Viviroli, D., Dürr, H., Messerli, B., Meybeck, M., and Weingartner, R.: Mountains of the world, water towers for humanity: Typology, mapping, and global significance, Water Resour. Res., 43, https://doi.org/10.1029/2006WR005653, 2007.

Zhang, Z., Glaser, S., Bales, R., Conklin, M., Rice, R., and Marks, D.: Insights into mountain precipitation and snowpack from a basin-scale wireless-sensor network, Water Resour. Res., 53, 6626–6641, https://doi.org/10.1002/2016WR018825, 2017.